

US-APWR

Reactor Vessel Lower Plenum 1/7 Scale Model Flow Test Report

Non-Proprietary Version

June 2008

**©2008 Mitsubishi Heavy Industries, Ltd.
All Rights Reserved**

(This page is intentionally blank)

Revision History

Revision	Date	Page	Description
0	June 2008	All	Original issued

© 2008

MITSUBISHI HEAVY INDUSTRIES, LTD.
All Rights Reserved

This document has been prepared by Mitsubishi Heavy Industries, Ltd. ("MHI") in connection with the U.S. Nuclear Regulatory Commission's ("NRC") licensing review of MHI's US-APWR nuclear power plant design. No right to disclose, use or copy any of the information in this document, other than by the NRC and its contractors in support of the licensing review of the US-APWR, is authorized without the expressed written permission of MHI.

This document contains technology information and intellectual property relating to the US-APWR and it is delivered to the NRC on the expressed condition that it not be disclosed, copied or reproduced in whole or in part, or used for the benefit of anyone other than MHI without the expressed written permission of MHI, except as set forth in the previous paragraph. This document is protected by the laws of Japan, U.S. copyright law, international treaties and conventions, and the applicable laws of any country where it is being used.

Mitsubishi Heavy Industries, Ltd.
16-5, Konan 2-chome, Minato-ku
Tokyo 108-8215 Japan

Abstract

The US-APWR reactor internals are designed for the 14-ft core of 257 fuel assemblies. This design is developed from J-APWR, which has 12-ft core. The US-APWR has the 14-ft core installed without changing the total height of the reactor vessel by consolidating the lower core plate into the lower core support plate (LCSP). While this type of LCSP design has already existed as a proven design for 14-ft core reactor in the US and in Europe, the LCSP with 257 fuel assemblies design is a new design. In addition, a simplified and symmetric design for the lower plenum internals is introduced due to applying upper in-core instrumentation system instead of bottom in-core instrumentation system.

This report documents the 1/7 scale model flow test for the reactor vessel lower plenum design. The test section simulated the lower portion of the US-APWR reactor internals, which included the inlet nozzle, downcomer, lower plenum and LCSP. The test was performed under the ambient temperature and pressure. This test was conducted to confirm the thermal hydraulic and flow-induced vibration (FIV) characteristics of the US-APWR lower plenum design, especially in the following areas:

(1) Hydraulic characteristics

- Flow stability
- Core inlet flow distribution
- Neutron reflector (NR) inlet flow distribution
- Pressure loss through the downcomer, the lower plenum and the LCSP

(2) FIV characteristics of the lower plenum structures

(3) Core inlet temperature distribution on an asymmetric loop cooling condition

From the test results, the following conclusions were obtained.

- The configured design of reactor vessel lower plenum with the diffuser plate assembly and LCSP flow holes provides the core inlet flow distributions at great flow stability.
- No abnormal vibration such as the lock-in vortex-induced vibration or the fluid elastic instability that is present in the components in the vessel lower plenum. The alternating stresses in the components are smaller than the design limit for the high cycle fatigue.
- The core inlet temperature distribution under asymmetric loop cooling conditions is bounded by the safety analysis model on the downcomer/lower plenum mixing.

Table of Contents

1. INTRODUCTION	11
1.1 Background	11
1.2 Reactor Design of the US-APWR.....	11
1.2.1 Design Concept	11
1.2.2 Lower Reactor Internals.....	11
1.3 Test Purpose	12
1.3.1 Hydraulic Characteristics	12
1.3.2 Flow- Induced Vibration	13
1.3.3 Temperature Distribution	14
2. OVERVIEW OF THE PROGRAM	21
2.1 Hydraulic Test.....	21
2.2 Flow-Induced Vibration Test.....	21
2.3 Core Inlet Temperature Distribution Test	22
3. TEST METHOD	23
3.1 Test Equipment	23
3.1.1 Test Loop.....	23
3.1.2 Vessel and Internals	23
3.2 Test Conditions.....	23
3.2.1 Flow Conditions	23
3.2.2 Scaling Rules.....	24
3.3 Measurements.....	25
3.3.1 Hydraulic Test.....	25
3.3.2 Flow-Induced Vibration Test.....	26
3.3.3 Core Inlet Temperature Distribution Test.....	26
3.4 Test Procedure	27
3.4.1 Hydraulic Test.....	27
3.4.2 Flow-Induced Vibration Test.....	28
3.4.3 Core Inlet Temperature Distribution Test.....	29
4. TEST RESULTS AND DISCUSSIONS	54
4.1 Hydraulic Test.....	54
4.2 Flow-Induced Vibration Test.....	56
4.3 Core Inlet Temperature Distribution Test	60
5. CONCLUSIONS	89
6. REFERENCES	90
APPENDICES	
Appendix-1: Response to the Request for Additional Information on US-APWR Vessel Lower Plenum 1/7 Scale Model Flow Test plan (UAP-HF-07080-P rev.0)	91
Appendix-2: Evaluation of Measurement Uncertainties	96

List of Tables

Table 3-1 Comparison of the Dimension of Test Model and Plant.....	30
Table 3-2 Coolant Flow Parameters	31
Table 3-3 Non-dimensional Parameters	32
Table 3-4 General Rule of Scaling Effect.....	33
Table 3-5 Correction Factors for the FIV Test.....	33
Table 3-6 Measurement Items for Hydraulic Test.....	34
Table 3-7 Measurement Items for Flow-Induced Vibration Test	35
Table 3-8 Measurement Items for Core Inlet Temperature Distribution Test.....	36
Table 3-9 Test Matrix with Number Runs and Test Conditions for Hydraulic Test	37
Table 3-10 Test Matrix with Number Runs and Test Conditions for Flow Induced Vibration	38
Table 4-1 Results of Core Inlet Flow Distributions (Test H3)	62
Table 4-2 Comparison of Core Inlet Flow Distribution between All Loop Operation and N-1 Loop Operation	63
Table 4-3 NR Flow Rate Distribution.....	64
Table 4-4 Natural Frequencies of Diffuser Plate Subassembly	65
Table 4-5 Natural Frequencies under Plant Operating Conditions	65
Table 4-6 Margins of Safety for Fluid-Elastic Instability	66
Table 4-7 Evaluation for Vortex Shedding Lock-in.....	66
Table 4-8 Section Modulus Ratio of Measurement Points and Evaluation Point.....	67
Table 4-9 Results of High Cycle Fatigue Evaluation.....	68

List of Figures

Figure 1-1 Comparison between the US-APWR and the Current 4-loop Plant.....	17
Figure 1-2 Reactor Internals General Arrangement.....	18
Figure 1-3 Main Core Cooling Flow and Bypass Flow	19
Figure 1-4 Lower Reactor Internals Assembly	20
Figure 3-1 Test Loop and Test Model.....	40
Figure 3-2 Scope of Simulation.....	41
Figure 3-3 Model of Reactor Vessel and Lower Internals (1/7 Scale Model).....	42
Figure 3-4 Hydraulic Test Measurement Block Diagram	43
Figure 3-5 PIV System.....	44
Figure 3-6 Measuring Locations of Transient History Flow Rate	45
Figure 3-7 Measuring Locations of Inlet Flow Distribution	46
Figure 3-8 Regions for NR Inlet Flow Evaluation	47
Figure 3-9 Measuring Locations of Pressure	48
Figure 3-10 Flow-Induced Vibration Measurement Block Diagram.....	49
Figure 3-11 Measuring Locations of Flow-Induced Vibrations	50
Figure 3-12 Measuring Locations of Core Inlet Temperature	51
Figure 3-13 Orifice Pattern of Inlet Flow Holes	52
Figure 3-14 Daily Check of Data Repeatability	53
Figure 4-1 Time-Averaged Velocity Map by PIV (without Diffuser Plate Assembly: Test H1)	69
Figure 4-2 Snap-Shots of Velocity Map by PIV (without Diffuser Plate Assembly: Test H1)	70
Figure 4-3 Time History of Flow Rate Distribution (without Diffuser Plate Assembly: Test H1).....	71
Figure 4-4 Time-Averaged Velocity Map by PIV (with Diffuser Plate Assembly: Test H2)	72
Figure 4-5 Snap-Shots of Velocity Map by PIV (with Diffuser Plate Assembly: Test H2)	73
Figure 4-6 Time History of Flow Rate Distribution(with Diffuser Plate Assembly: Test H2)	74
Figure 4-7 Time-Averaged Velocity Map by PIV(with Diffuser Plate Assembly and Design LCSP Flow Hole Pattern: Test H3).....	75
Figure 4-8 Snap-Shots of Velocity Map by PIV(with Diffuser Plate Assembly and Design LCSP Flow Hole Pattern: Test H3).....	76
Figure 4-9 Time History of Flow Rate Distribution (with Diffuser Plate Assembly and Design LCSP Flow Hole Pattern: Test H3).....	77
Figure 4-10 Core Inlet Flow Distribution (without Diffuser Plate Assembly: Test H1).....	78
Figure 4-11 Core Inlet Flow Distribution (with Diffuser Plate Assembly: Test H2, []).....	79
Figure 4-12 Core Inlet Flow Distribution (with Diffuser Plate Assembly and Design LCSP Flow Hole Pattern: Test H3, []).....	80
Figure 4-13 Core Inlet Flow Distribution (with Diffuser Plate Assembly and Design LCSP Flow Hole Pattern: Test H3, []).....	81
Figure 4-14 Core Inlet Flow Distribution (with Diffuser Plate Assembly and Design LCSP Flow Hole Pattern: Test H3, N-1 Loop).....	82
Figure 4-15 Measured Pressure Losses (Dependency with Re Number: Test H3).....	83

Figure 4-16 Measuring and Tapping Locations and Reference of Mode Shape.....	84
Figure 4-17 Natural Frequencies and Vibration Mode Shapes	85
Figure 4-18 Flow Rate Dependency of Vibration Response	86
Figure 4-19 Core Inlet Non-dimensional Temperature Distribution.....	87
Figure 4-20 Safety Analysis Model for Core Inlet Temperature Distribution	88
Figure 4-21 Comparison of Core Inlet Temperature Distribution between Design Model and Flow Test	88

List of Acronyms

APWR	Advanced Pressurized Water Reactor
ASME	American Society of Mechanical Engineers
DNB	Departure from Nucleate Boiling
FIV	Flow-Induced Vibration
LCSP	Lower Core Support Plate
MDF	Mechanical Design Flow
NR	Neutron Reflector
PIV	Particle Image Velocimetry
PWR	Pressurized Water Reactor
rms	Root Mean Square
TDF	Thermal Design Flow

1. INTRODUCTION

1.1 Background

The US-APWR reactor internals were designed with a 14-ft core to contain 257 fuel assemblies. This design was developed from the J-APWR, which has a 12-ft core. The US-APWR accommodates the 14-ft core with no change in the total height of the reactor vessel by consolidating the lower core plate into the lower core support plate (LCSP). While this LCSP is already a proven design for 14-ft core reactors in the US and in Europe, a LCSP with 257 fuel assemblies design is a new design feature. Additionally, a simplified and symmetric design for the lower plenum internals was introduced due to applying upper mounted incore instrumentation system instead of bottom mounted incore instrumentation system.

MHI has accumulated experiences in the reactor vessel lower plenum design including the LCSP through several flow tests. These experiences are beneficial to the US-APWR design involving the core inlet flow distribution, flow stability in the lower plenum, and thermal mixing effects. They are thus used as part of the design accommodation for reliability purpose. To assure the reliability of the design, a confirmation test was conducted for the US-APWR design.

A 1/7 scale model flow test was carried out for the lower plenum of the reactor vessel. This test was conducted to confirm the thermal hydraulic and flow-induced vibration characteristics in the lower plenum of the US-APWR. The schedule of this test is shown in Table 1-1.

1.2 Reactor Design of the US-APWR

1.2.1 Design Concept

The design concept of the US-APWR reactor is a progressive evolution from the current 4-loop plants. Comparison of the reactor vessel and internals between the US-APWR and the current 4-loop plants is shown in Figure 1-1. The primary reactor design parameters of the US-APWR (Ref.1) are compared with those of the current 4-loop plants as shown in Table 1-2.

The general arrangement of the US-APWR reactor internals is shown in Figure 1-2. The US-APWR reactor internal components evolved from the proven 4-loop plant design currently operating in the US and in Japan. The differences are as follows;

- Design: A neutron reflector instead of baffle structures to enclose the core, and a simplified and symmetric diffuser plate assembly for the lower plenum structures.
- Size: Increases in the diameters of the reactor vessel, core barrel and the lower plenum structures.

Flow paths in the US-APWR reactor, as shown in Figure 1-3, are similar to those in the current 4-loop plants.

1.2.2 Lower Reactor Internals

The lower reactor internals assembly is shown in Figure 1-4.

(1) Core barrel / lower core support plate

The diameter of the core barrel in the US-APWR is about twenty percent larger than that in the current 4-loop plants in order to accommodate the increase in the number of fuel assemblies from 193 to 257 to obtain a larger thermal output.

The fuel assemblies are secured on the LCSP at the bottom of the core barrel with the hold down springs. The LCSP has four flow holes for each of the 257 fuel assemblies. The flow hole has an orifice to control the core inlet flow distribution.

(2) Neutron reflector

The neutron reflector (NR) is a new component instead of using the baffle structures. It consists of the perforated metal blocks and forms the core cavity. Flow holes of the NR metal blocks are needed to remove the heat generated inside the blocks. The NR coolant flow goes through inlet holes located in the peripheral region of the LCSP from the RV lower plenum to the NR lower plenum. The NR cooling flow is redistributed in the NR lower plenum by the inlet orifices of the NR bottom block flow holes.

(3) Lower plenum structures

The diffuser plate assembly is placed in the lower plenum of the US-APWR. This assembly consists of two subassemblies. The upper subassembly consists of one ring diffuser plate and eight support columns. The lower subassembly consists of one circle diffuser plate which has several flow holes, twelve support columns and extension tubes, four secondary core support columns, energy absorbers, and a base plate. These assemblies are connected to the bottom surface of the LCSP. This configuration is similar to the tie plates and the bottom mounted instrumentation columns in the current 4-loop plant. But the diffuser plate assembly is simplified and symmetrically designed comparing with the lower plenum structures of the current plant, because the guides for the bottom mounted instrumentation are no longer necessary.

1.3 Test Purpose

1.3.1 Hydraulic Characteristics

One of the purposes of this test program is to confirm that the components of the lower reactor internals are designed to provide stable flow into the core and consequently no adverse local flow conditions are prepared at the core inlet.

a. Flow stability

The diffuser plate assembly was designed to stabilize the lower plenum flow. To confirm the effect of the diffuser plate assembly, flow conditions were observed for two different configurations, with and without the diffuser plate assembly. An anticipated result in the case with the diffuser plate assembly is that no unstable flow occurred.

b. Core inlet flow distribution

The core inlet flow distribution may affect core cooling, vertical hydraulic load on the fuel assemblies, and cross-flows among the fuel assemblies. The test was conducted to confirm that the inlet flow distribution satisfy the following targets. They were not design criteria, but were established as design guidance based on the former test experiences. If the test results showed any of the design targets (or guidance) was not met, the effect on the design margin would be evaluated.

- Minimum fuel assembly flow rate
Reduction in the hot assembly flow can affect the DNB design. It was conservatively established that the minimum fuel assembly flow rate should be no smaller than [] percent of the core averaged flow rate. Since the core inlet flow is immediately re-distributed in the lower region of the core, the inlet flow maldistribution will have negligibly small effect on the DNB design.
- Maximum fuel assembly flow rate
Large fuel assembly flow may have an affect on the designed hold-down spring of fuel assembly due to the increase in the vertical hydraulic load. Based on experiences of the previous tests, it was conservatively established that the maximum of fuel assembly flow rate should be no greater than [] percent of the core averaged flow rate.
- Maximum differential flow rate between adjacent fuel assemblies
Cross-flows caused by differential flow rates between adjacent fuel assemblies have an effect on the flow-induced vibration of the fuel rods. Based on experiences of the previous tests, it was conservatively established that the maximum of differential flow rate between adjacent fuel assemblies should be no greater than [] percent of the core averaged flow rate.

c. NR inlet flow distribution

Reduction in the NR coolant flow rate has an effect on the temperature of the NR blocks. The circumferential and radial pressure distribution below the LCSP would affect to the NR inlet flow rate distribution.

The test was conducted to confirm the inlet flow distribution. The inlet flow distribution is expected to be redistributed in the NR lower plenum. However, this effect is not considered and it was conservatively established that the minimum NR coolant flow rate should be no less than [] percent of the estimated value. This target would be met for [] .

The details of the sectors and the areas are discussed in subsection 3.3.1. If the test results did not meet the design target, the effect on the design margin would be evaluated.

d. Pressure loss

The pressure loss data are measured in this test program. They are used for confirming that the test is properly performed.

1.3.2 Flow- Induced Vibration

The components in the lower plenum could be damaged by flow-induced structural vibration. This test was conducted to confirm the structural integrity of these components with the following design targets.

a. Abnormal vibrations

No fluid elastic instability or rock-in vortex induced vibration is present.

b. High-cycle fatigue

The alternating stress amplitudes in the structures do not exceed the design limit for the high-cycle fatigue based on the ASME code design fatigue curve (Ref. 2).

1.3.3 Temperature Distribution

In the safety analysis, the coolant temperature mixing in the downcomer / lower plenum was modeled for an asymmetric loop cooling condition. This test was conducted to confirm that the safety analysis model was adequate for the core inlet temperature distribution.

Table 1-1 Schedule of Reactor Vessel Lower Plenum 1/7 Scale Model Flow Test

Year	2007										2008		
Month	4	5	6	7	8	9	10	11	12	1	2	3	
Test Plan (2006/9-10)													
Equipment Design (2006/11-2007/4)	█												
Existing Facility Inspection and Maintenance			█	█	█	█	█	█	█				
Manufacturing & Setting				█	█	█	█	█	█				
Hydraulic Test - Measurement System Set Up - Test without Diffuser Plate Assembly - Test with Diffuser Plate Assembly - Test with Diffuser Plate Assembly and Configured LCSP Design							█	█	█	█			
FIV Test -Measurement System Set Up -Test										█	█		
Core Inlet Temperature Distribution Test -Measurement System Set Up -Test											█	█	

Table 1-2 Comparison of Principal Reactor Design Parameters

Parameter	US-APWR	Typical 12-ft 4-loop PWR	Typical 14-ft 4-loop PWR
Key Reactor Parameters			
Core Thermal Output (MWt)	4451	3565	3853
System Pressure (psia)	2250	2250	2250
Inlet Temperature (°F)	550.6	556.8	549.8 to 561.2
Core Average Temperature (°F)	588.8	592.2	586.9 to 597.8
Vessel Average Temperature (°F)	583.8	588.4	582.3 to 593.8
Vessel Thermal Design Flow (10 ⁶ lbm/hr)	168.2	139.4	145.0
Core Bypass Flow (%)	9.0	6.4	8.5
Reactor Structural Parameters			
Equivalent Core Diameter (ft)	12.8	11.1	11.1
Thermal Shield/Reflector Design	Neutron Reflector	Neutron Panel	Neutron Pad
Core Barrel ID/OD (in)	175.98/181.97	148.0/152.5	148.0/152.5
Fuel Parameters			
Number of Fuel Assemblies	257	193	193
Fuel Assembly Array	17x17	17x17	17x17
Number of Fuel Rods	264	264	264
Effective Fuel Length (in)	165.4	143.7	168

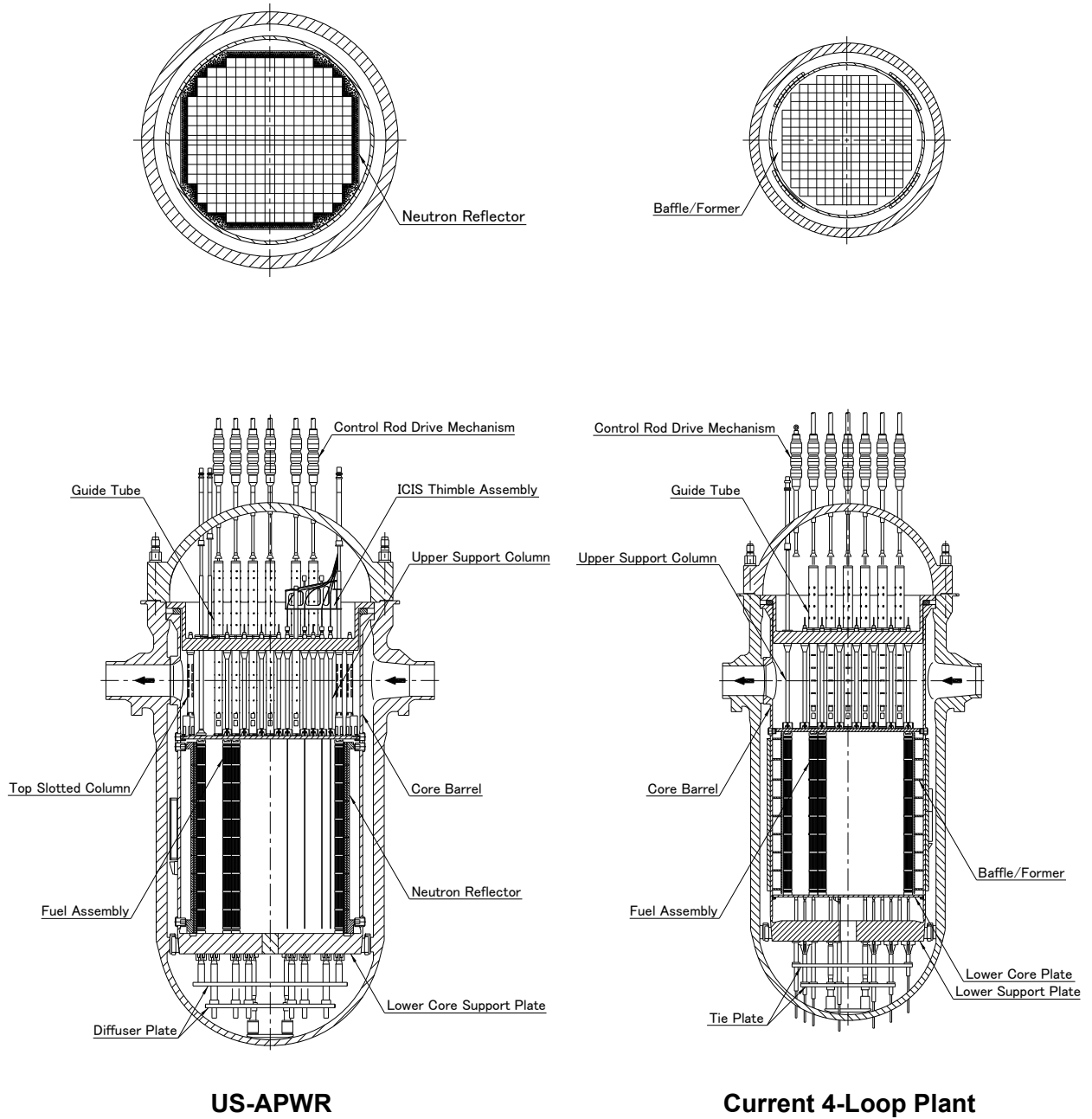


Figure 1-1 Comparison between the US-APWR and the Current 4-loop Plant

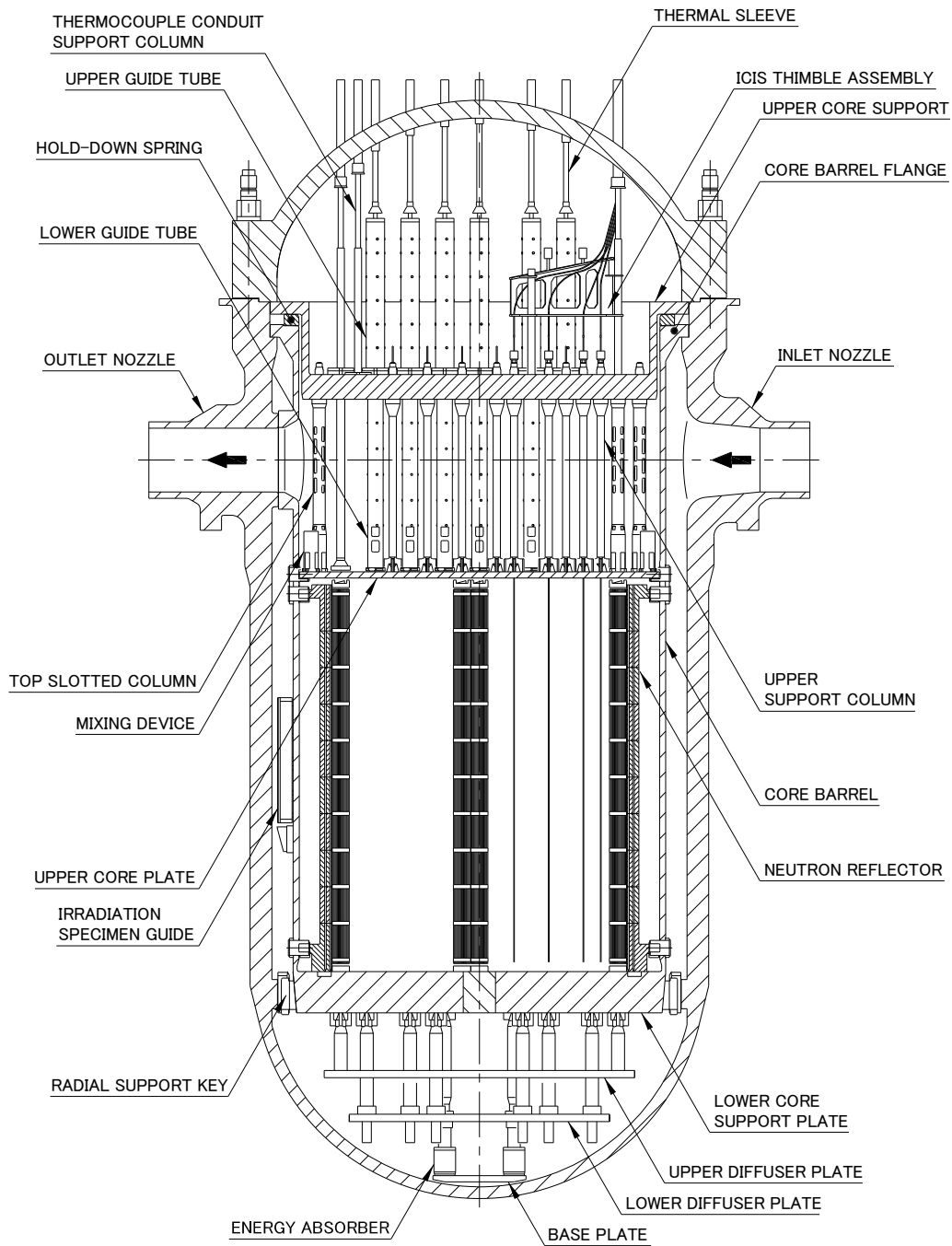


Figure 1-2 Reactor Internals General Arrangement

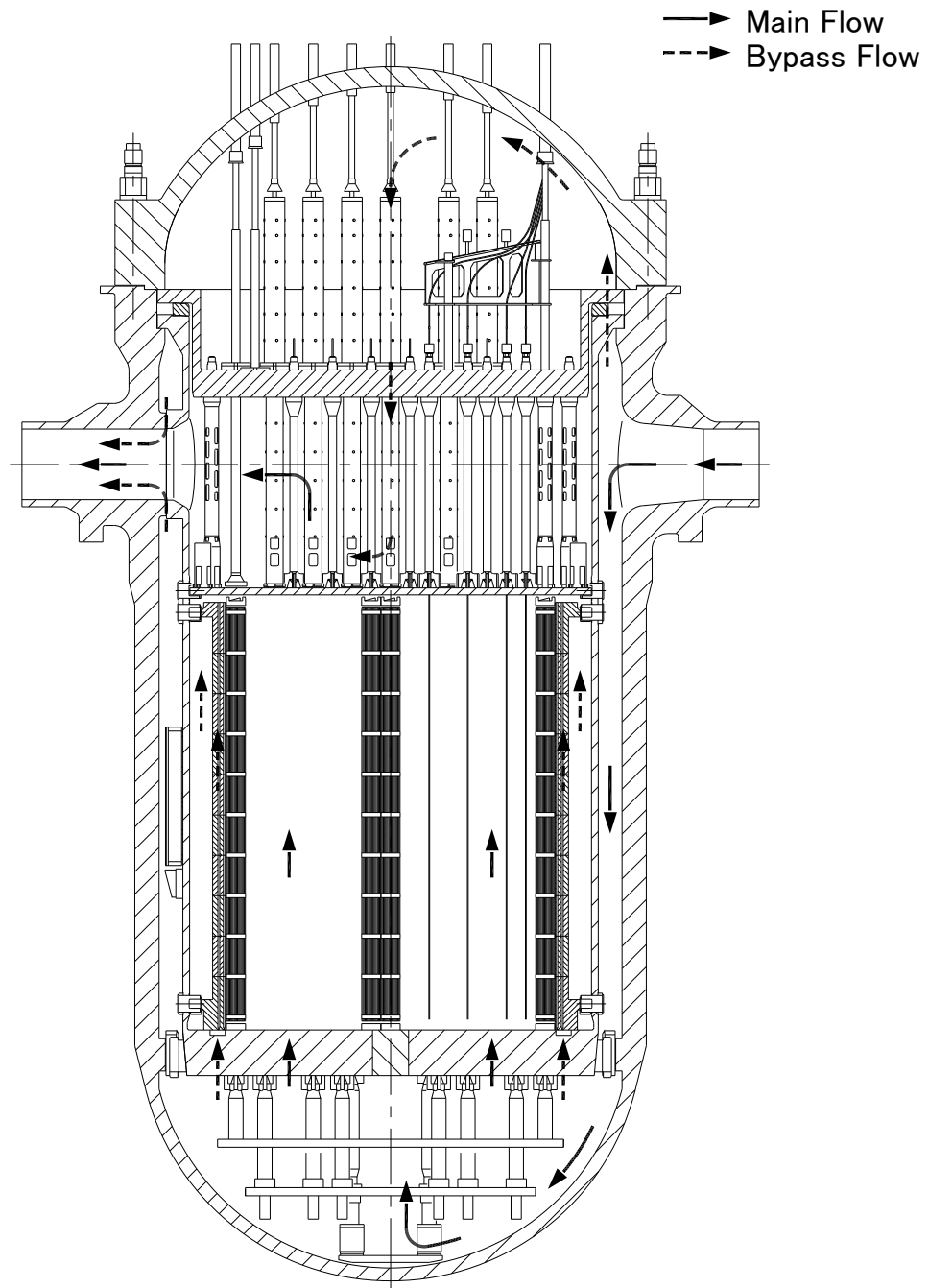


Figure 1-3 Main Core Cooling Flow and Bypass Flow

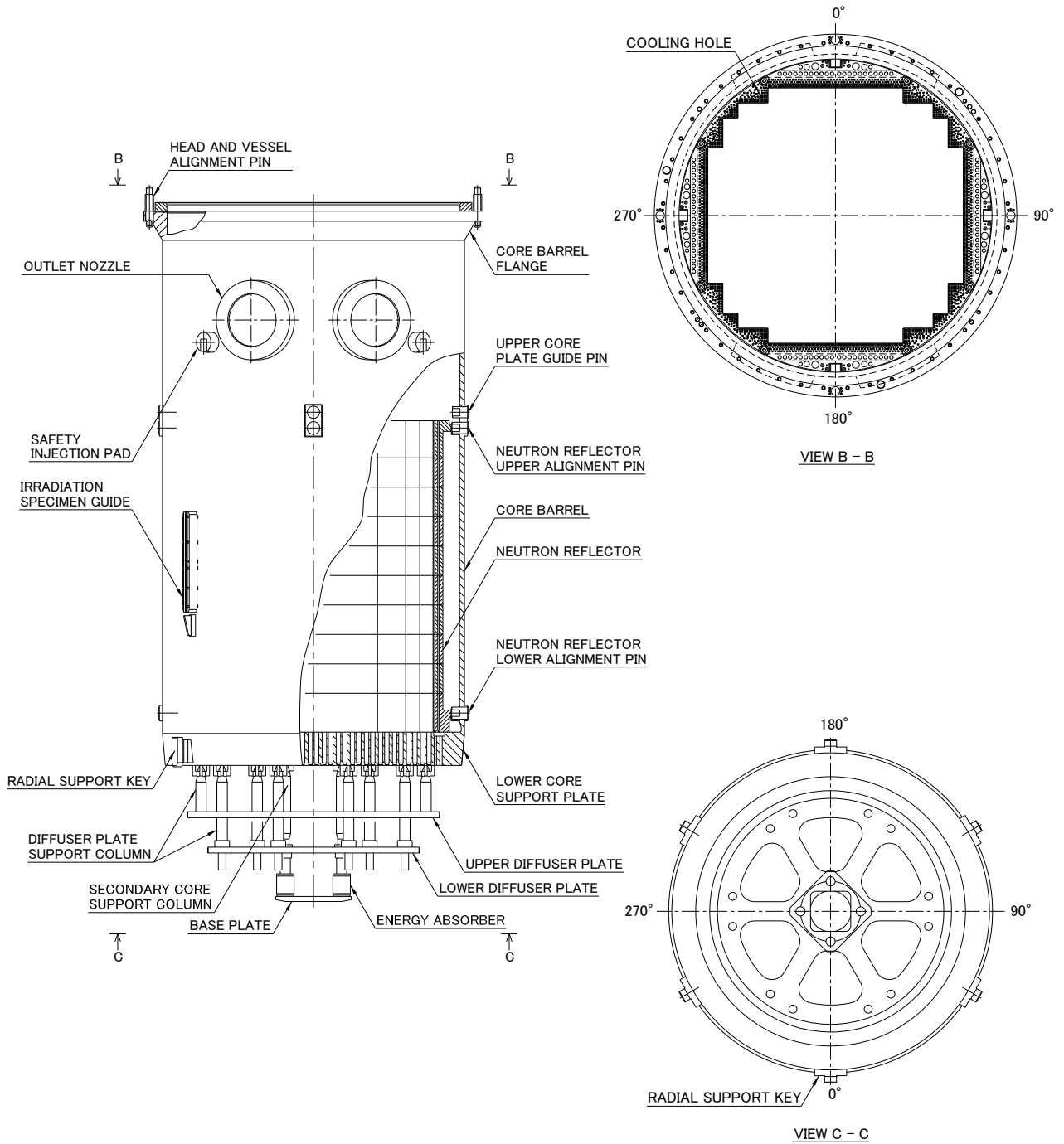


Figure 1-4 Lower Reactor Internals Assembly

2. OVERVIEW OF THE PROGRAM

Three types of flow tests were performed using the 1/7 scale model to verify the design, as discussed above. The test section simulated the lower portion of the US-APWR reactor internals, which includes the inlet nozzles, the downcomer, the lower plenum and the lower core support plate (LCSP). All tests were performed at room temperature and atmospheric pressure.

2.1 Hydraulic Test

The purpose of the hydraulic test is to confirm that the lower reactor internals provide sufficiently stable and uniform flow into the core. The following items were studied:

a. Flow stability

The velocity field in the lower plenum was observed by the particle image velocimetry (PIV) methodology and the time histories of the core inlet flow rates were measured by Venturi flow meters at the LCSP flow holes. These measurements confirmed the flow stability in the lower plenum and with the core inlet flow rates. The diffuser plates assembly was designed to stabilize the flow in the lower plenum. The measurement was conducted both with and without the diffuser plate assembly.

b. Core inlet flow distribution

One Venturi flow meter was installed in []. A total of [] Venturi flow meters were used to measure the core inlet flow distribution. The test was conducted simulating the full flow conditions of the plant. The results were confirmed to meet the target. The condition at N-1 loop operation was also measured, even though the US-APWR was not designed to operate in this mode.

c. NR Inlet flow distribution

The [] Venturi flow meters were installed on periphery of the core to measure the NR inlet flow distribution. The measured data were reduced to []. The details of the sectors and the areas are discussed in subsection 3.3.1. The data showed that the NR inlet flow rate was less than the target. However, the effect for the NR metal block temperature is small, and the effect on the design margin would be evaluated.

d. Pressure loss

The static pressure taps were installed on several locations along the flow path. The pressure losses through the downcomer, lower plenum and LCSP were measured. It was confirmed that the test section design and the test operation were properly conducted.

2.2 Flow-Induced Vibration Test

The purpose of the flow-induced vibration test is to confirm the structural integrity of the components in the lower plenum. Accelerometers were mounted on the diffuser plates to measure the vibration characteristics (natural frequencies). Strain gauges were installed on the support columns to measure the dynamic strains (alternating stresses).

The possibility of abnormal vibrations, such as the lock-in vortex induced vibration or fluid-elastic instability, was evaluated from the relationship between flow rates and the vibration responses. The safety margins for high cycle fatigue were confirmed by the alternating stresses.

2.3 Core Inlet Temperature Distribution Test

The purpose of the core inlet temperature distribution test was to confirm the mixing characteristics in the downcomer and in the lower plenum. The core inlet temperature distribution was measured with [] uniformly distributed thermocouples (TCs). Through one of the cold legs, hot water was injected into the reactor vessel to simulate the asymmetric cooling event. The results were compared with the safety analysis model and were confirmed to be properly modeled in the safety analyses.

3. TEST METHOD

3.1 Test Equipment

3.1.1 Test Loop

The primary cooling system of the US-APWR has a 4-loop configuration. The test loop was consisted of the inlet and outlet pipes, pumps and a waterpool as shown in Figure 3-1.

3.1.2 Vessel and Internals

Four sets of the inlet and outlet nozzles, the lower part of the reactor vessel and the downcomer were modeled in the test section as shown in Figure 3-2.

The maximum flow rate in the test was determined taking into consideration the temperature difference between the test and the actual plant operating conditions. The limitation in the test loop flow rate was also taken into consideration in determining the scale of the test section. To simulate the hot operating condition of the reactor, a 1/7 scale model was selected for the test model. Detailed discussion of the scaling rule is presented in subsection 3.2.2.

The reactor vessel and the lower reactor internals are shown in Figure 3-3. Comparisons of the dimensions between the actual plant and the test model are shown in Table 3-1. The lower head of the test vessel was made of the acrylic resin to provide flow visualization. The outlet nozzle simulated only the nozzle blockage in the downcomer as shown in Figure 3-3. The pressure losses of the fuel assemblies were simulated by a perforated plate and measured with Venturi flow meters.

The test vessel was set in an upside down position for easy access to install the measuring devices and for flow visualization using PIV. This inverted position has no effect on the flow simulation, because the flow inside a reactor vessel of PWR is of forced convective type without any free surfaces. The buoyancy effect on thermal mixing of coolant is negligible of described in subsection 3.2.2. Therefore, the effect of gravity is negligible.

3.2 Test Conditions

This test was conducted at room temperature and atmospheric pressure using the 1/7 scale model. Flow conditions and scaling rules are discussed in the following.

3.2.1 Flow Conditions

The thermal design flow (TDF) rate and mechanical design flow (MDF) rate of the US-APWR plant are 112,000 gpm and 130,000 gpm per loop, respectively. In this test, a scaling law is used to determine the flow rates in the test that would simulate the design flow rates.

In the hydraulic test, the nominal flow rate in the loop was determined to be [] gpm to maintain the dynamic pressure under plant operating conditions at the thermal design flow rate. In the flow-induced vibration test, the nominal flow rate in the loop was determined to be [] gpm to maintain the reduced velocity ($U/(fnD)$) under the plant operating conditions at the mechanical design flow rate.

The coolant flow parameters in this test are shown in Table 3-2.

3.2.2 Scaling Rules

Taking into consideration the fabrication of the test model, the measurement and the capability of the test loop flow, the dimensions of the test model were selected to be 1/7 scale of the actual plant. The conditions were determined by performing the following non-dimensional analyses. The selected key dimensionless parameters for each test item were determined as shown in the Table 3-3 and as discussed below.

a. Hydraulic test

Under operating conditions of the US-APWR, the coolant flow inside the reactor vessel will be in the turbulent flow regime. It is considered that the flow characteristics would remain the same in sufficiently developed turbulent flow regime. The transition from laminar flow to turbulent flow occurs at Reynolds number ($Re = UD/\nu$) around 10^3 as described in Reference 3. For this reason, we selected the test condition to keep Re greater than 10^4 .

Under nominal conditions in the hydraulic test, Re in the downcomer was 2×10^5 . It remained above 10^5 even under minimum flow conditions. These numbers were sufficiently large to simulate the well-developed turbulent flow conditions. The computed Re in the actual plant and under the test conditions are summarized in Table 3-3.

b. Flow-induced vibration test

Several non-dimensional parameters, such as the Reynolds number, reduced velocity and Strouhal number, should be considered in planning flow-induced vibration test.

The requirements in Re was also considered in the flow-induced vibration test.

The reduced velocity ($U_r = U/(fnD)$) is generally utilized in the dimension analysis of the flow-induced vibration. U_r represents the ratio of the path length per cycle (U/fn) and the model width (D) as described in Reference 4. From another view point, U_r represents the ratio of the fluid force frequency (proportional to U/D , the vortex shedding frequency (f_s) is a typical example) to the natural frequency of the model. The nominal flow rate in the test should be determined so that U_r coincides with that of the plant. If the test model is precisely scaled down, fnD is maintained. Therefore, for U_r to be the same as in the plant, the velocity in the test should be the same as that in the plant. The computed U_r in actual plant as well as that under the test conditions are summarized in Table 3-3. Scaling effects for the physical parameters of test model are shown in Table 3-4.

The Strouhal number ($St = f_s D/U$) is the non-dimensional parameter for the vortex shedding frequency (Ref.5). St of a cylinder in cross-flow depends on Re . St under plant operating conditions will be [] percent higher than that under the test conditions due to the difference in Re . The maximum flow rate for the flow-induced vibration test was selected to be [] percent of the mechanical design flow rate. The ratio of vortex shedding frequency to the natural frequency of the structures under plant operating conditions was maintained during the test.

The effects of temperature on the flow-induced responses were considered from the view point of flow-induced forcing functions and the stiffness of the structure. The main sources of the flow-induced vibration are the turbulent pressure fluctuation and the vortex shedding. The amplitudes of these forcing functions are proportional to the dynamic pressure ($1/2 \rho U^2$). Thus, the temperature effect on the flow-induced forces can be related to the change in the fluid mass density. The temperature effect on the stiffness of the structure can be estimated from the ratio of the Young's moduli of the material at different temperatures. Therefore, the effects of temperature on vibration response were adjusted with the differences in fluid mass densities and Young's moduli. The correction factors were used to translate the test results into corresponding values under actual operating conditions considering the scale and temperature effects. These numbers are summarized in Table 3-5.

c. Temperature distribution test

The Richardson number (Ri) is a non-dimensional parameter that represents the ratio of buoyancy and fluid inertia forces as described in Reference 6. It is considered that the buoyancy effect on thermal mixing of coolant is negligibly small when Ri is much smaller than 1, Table 3-3 shows Ri of both the actual event and the test conditions.

3.3 Measurements

3.3.1 Hydraulic Test

The components of the lower reactor internals were designed to provide sufficiently stabilized flow into the core and consequently no adverse local flow conditions. The following four kinds of measurements were performed in the hydraulic characteristics test. The block diagram for the measurements in the hydraulic test is shown in Figure 3-4. Items measured in the hydraulic test are shown in Table 3-6.

a. Flow stability

The flow velocity field in the lower plenum was measured by the PIV method. The PIV system was set on the test vessel bottom head as shown in Figure 3-5. Laser sheet was injected horizontally to the lower plenum. Velocity vectors were obtained from particle movement in the coolant. Flow velocity vector maps were developed by the computer system from the test results. In addition, the selected [] Venturi flow meters were used to measure transient history as shown in Figure 3-6. The block diagram for the local flow rate measurement is shown in Figure 3-6.

b. Core inlet flow distribution

The core inlet flow rates were measured by the Venturi flow meters at [] locations as shown in Figure 3-7. The core inlet flow distribution was generated by the time-averaged measurement data.

c. NR inlet flow distribution

The NR inlet flow rates were measured by the Venturi flow meters at the [] peripheral

regions outside of the core as shown in Figure 3-7. The measured data were used to evaluate the NR inlet flow rate distribution. It is worth noting that the reduction of the NR inlet flow rate due to the pressure distribution below the LCSP might affect to the cooling capability.

[

Figure 3-8. The [] are compared with the design target presented in subsection 1.3.1.

d. Pressure loss

Pressure losses along the main flow path from the inlet nozzle of the reactor vessel up to the simulated core outlet were measured using static pressure taps as shown in Figure 3-9. Pressure taps were connected to the pressure transducers to generate electric signals for the computer system. Time-averaged data were used for calculating the pressure losses.

3.3.2 Flow-Induced Vibration Test

The vibration characteristics and the alternating stresses were evaluated to confirm the integrity of the components in the lower plenum. The alternating stresses are caused by flow-induced vibration loads. The vibration characteristics such as the natural frequencies and mode shapes were evaluated from the acceleration data. The alternating stresses were obtained from the strain data. The block diagram for the vibration test measurements is shown in Figure 3-10.

a. Vibration characteristics

The acceleration responses were measured by the accelerometers as shown in Figure 3-11 and Table 3-7. [

] The types and locations of the sensors used in the flow-induced vibration measurement are summarized in Table 3-7.

b. Components integrity

The strains in the components were measured by the strain gauges as shown in Figure 3-11 and Table 3-7. [

] The alternating stresses were deduced from the time histories of the strain data. The pressure fluctuations were measured with dynamic pressure transducers as reference information for the flow loads as shown in Figure 3-9 and Table 3-7. This information could be used for future developments.

3.3.3 Core Inlet Temperature Distribution Test

The core inlet temperature distribution test was conducted to confirm the mixing characteristics in the downcomer and in the lower plenum. The core inlet temperature distribution was measured by the uniformly distributed [] thermocouples (TCs). In addition, the coolant temperature was measured at the inlet nozzle. From these data, the mixing characteristics were evaluated. The arrangement of the TCs is shown in Figure 3-12 and Table 3-8.

3.4 Test Procedure

3.4.1 Hydraulic Test

As shown in Figure 3-13, the three steps in the test were performed to confirm the hydraulic performance of the diffuser plate assembly and the configured orifice pattern of the inlet flow holes of the LCSP. The test matrices including the test identification numbers (Test ID), test items and test conditions are shown in Table 3-9.

(1) Calibration and validation check

a. Pre-test work

The discharge coefficient for each Venturi flow meter was determined by a calibration test prior to the installation of the Venturi in the test vessel. All transducers and measuring systems were calibrated prior the tests.

b. Daily work

A repeatability test run was conducted on each day of testing. This test run was conducted following the last test of the day. These procedures were followed on each day of testing. The procedure is described in Figure 3-14.

(2) Test H1-Test without diffuser plate assembly

Test H1 was performed without the diffuser plate assembly. The orifice diameters of all the LCSP core inlet flow holes were uniform. The PIV method was used to observe the flow pattern in the lower plenum. The time histories of the core inlet flow rates were also measured with [] Venturi flow meters. The flow distribution was measured using [] Venturi flow meters. Data from successive tests were compared to evaluate the performance of the diffuser plate assembly. This test was performed at [] flow rate condition.

(3) Test H2-Test with diffuser plate assembly

Test H2 was conducted with the diffuser plate assembly in the lower plenum. The orifice sizes were identical to those in the Test H1. The same test procedures were repeated as for the test without diffuser plate assembly. To confirm the performance of the assembly in ensuring flow stability, the PIV and time history of inlet flow rate were recorded. The core inlet flow distributions were measured using [] Venturi flow meters. This test category was performed at [] flow rate conditions.

(4) Test H3-Configured design test

Test H3 was performed to confirm the performance of the configured design. Both the diffuser plate assembly and the configured LCSP with the optimized diameters of distributed orifice holes were used. [

] The core inlet flow distribution and the pressure loss of the configured design of LCSP were confirmed in this test.

3.4.2 Flow-Induced Vibration Test

This test was performed to confirm the mechanical integrity of the diffuser plate assembly. The test cases are shown in Table 3-10.

(1) Calibration and validation check

The relationships between the static loads on the diffuser plates and the strains in the columns were measured prior the test. The validations of the sensors were completed within each test day following the procedures shown in Figure 3-14.

(2) Tapping test

Free vibration tests were carried out by hand tapping the diffuser plate support columns with a hammer and the data was measured with accelerometers. The natural frequencies and vibration modes of the diffuser plate assembly were evaluated based on the measured data. These tapping tests were performed both in air and in water. The differences in the natural frequencies were used to derive the hydrodynamic mass to confirm the design.

(3) Flow test

a. Abnormal vibrations

Flow-induced vibration responses of components were measured by the strain gauges. The tests were performed at flow rates that gave flow velocities equal to [] of the mechanical design flow rate. From the time histories of the strain data, the root mean square (rms) values of the vibration responses were derived under each of the flow conditions.

The relationships between the flow rates and the rms values of vibration responses were studied. Absence of abnormal vibration was confirmed when the rms responses were proportional to the square of the flow rate.

b. High cycle fatigue

The 0-peak amplitude of the alternating stress in the test model was derived by multiplying the measured rms strain with the peak factor (ratio of peak amplitude to rms amplitude) and the Young's modulus at the test temperature. This amplitude was adjusted into 0-peak stress in the plant by considering the difference in the fluid mass densities, the section moduli, and the stress concentration factors. In addition, the differences in the Young's moduli in the test and in the actual plant operating temperatures were also considered.

From the calculations mentioned above, the amplitudes of the alternating stress intensity were obtained. These amplitudes were compared with the allowable amplitude for 10^{11} cycles based on the ASME code section III design fatigue curve (Ref.2).

3.4.3 Core Inlet Temperature Distribution Test

(1) Calibration and validation check

Prior to the installation into the vessel, all thermocouples were calibrated. The validation of thermocouples was done on each day of testing with a standard thermometer.

(2) Measurement of temperature distribution at core inlet

To simulate a non-uniform cooling condition among the primary loops, the hot water was supplied to one of the loops, while the rest of the loops provided with the water at room temperature. The temperature distribution at the core inlet was measured with the thermocouples which were distributed over the core. The conditions used for the test case are summarized in Table 3-11. Measured data were available after the temperature distribution reached the steady state. The test was conducted by the following steps.

- (i) Hot water was heated in the water tank prior to test operation.
- (ii) Pumps were started up and hot water of one loop and room temperature water of other loops were supplied to reactor vessel.
- (iii) At the same time with (ii), instrumentation system was set to be active.
- (iv) Measurement was continued until the hot water tank became empty.

Table 3-1 Comparison of the Dimension of Test Model and Plant

	Actual Plant	Test Model	Scale Ratio
Inlet Loop Diameter (in)))	1/7
Distance From Inlet Nozzle Center to Core Barrel Bottom (in)			1/7
Vessel Inside Diameter (in)			1/7
Core Barrel Outer Diameter (in)			1/7
LCSP Flow Holes to the Core Numbers Diameter (in)			1/7
Diffuser Plate Assembly Support Columns Numbers Diameter (in)			1/7
			(

Table 3-2 Coolant Flow Parameters

	Actual Plant	Hydraulic Test	FIV Test
Temperature (°F)	TDF: 550.6 ()	Approx. 70	Approx. 70
Pressure (psia)	2,250	[]	[]
Density (lb/ft ³)	TDF: 46.8 ()		
Nominal Loop Flow Rate (gpm)	TDF 112,000 MDF 130,000		

Table 3-3 Non-dimensional Parameters

	Key Parameter	Bases	Test Requirement	Plant Condition (Approx.)	Test Condition (Approx.)
Hydraulic Test	Reynolds Number ($Re = UD_1 / \nu$)	Ratio of Fluid Inertial Force and Viscous Force	$Re \gg 10^4$ (for Fully Developed Turbulent Flow)		
FIV Test	Reduced Velocity ($U_r = U / f_n D_2$)	Ratio of "Path Length per Cycle" and "Model width"	Equivalent with Plant Condition		
	Strouhal Number ($St = f_s D_2 / U$)	Ratio of "Vortex Shedding Frequency" and "Flow Velocity Divided by Cylinder Diameter"	Flow Velocity is Determined Considering the Ratio of St between Plant and Test		
Temp. Distribution Test	Richardson Number ($Ri = gD_1(\delta\rho) / \rho U^2$)	Ratio of Buoyancy and Fluid Inertia Force	Equivalent with Plant Condition or $Ri \ll 1.0$ for Test and Plant		

- U : flow velocity (= downcomer average velocity)
- D_1 : typical length of the flow path (= downcomer width)
- D_2 : typical length of the structure (= diameter of diffuser plate support column)
- ν : kinematic viscosity
- f_n : natural frequency
- f_s : vortex shedding frequency
- g : gravity acceleration
- ρ : fluid mass density
- $\delta\rho$: difference of mass density between cold fluid and hot fluid

Table 3-4 General Rule of Scaling Effect
(Scale= 1/N, Flow velocity is maintained)

	Dimension Analysis	General Scale Effect	Ratio in This Test
Length	L	1/N	1/7
Mass	M	1/N ³	1/343
Time	T	1/N	1/7
Area	L ²	1/N ²	1/49
Volume	L ³	1/N ³	1/343
Velocity	LT ⁻¹	1/1	1/1
Dynamic Pressure & Pressure Loss	ML ⁻¹ T ⁻²	1/1	1/1
Hydraulic Force	MLT ⁻²	1/N ²	1/49
Stress	ML ⁻¹ T ⁻²	1/1	1/1
Strain	1	1/1	1/1
Natural Frequency	T ⁻¹	N	7
Displacement	L	1/N	1/7
Acceleration	LT ⁻²	N	7

Table 3-5 Correction Factors for the FIV Test

	Correction for Fluid Mass Density	Correction for Young's Modulus	Correction for Scale	Total Correction Factor
Hydraulic Force	[]	Not Effective	49	[]
Strain	[]	[]	1	[]
Stress	[]	Not Effective	1	[]

Table 3-6 Measurement Items for Hydraulic Test

Measurement Item	Instrumentation	Locations	Number
Horizontal Flow Velocity Map	PIV	Lower Plenum	-
Core Inlet Flow Distribution	Venturi	see Figure 3-7	
NR Inlet Flow Distribution	Venturi	see Figure 3-7	
Pressure Loss	Static Pressure Taps	see Figure 3-9	

Table 3-7 Measurement Items for Flow-Induced Vibration Test

Measurement Item	Measuring Parts	Measuring Location	Sensing Direction	Sensor ID	Number of Sensors
Strain	Upper Diffuser Plate Support Column (LCSP Side)				
	Lower Diffuser Plate Support Column (LCSP Side)				
	Column Extension (Fix End)				
	Secondary Core Support Column (LCSP Side)				
Acceleration	Upper Diffuser Plate				
	Lower Diffuser Plate				
	Base Plate				
	Core Barrel				
	Reactor Vessel				
Pressure Fluctuation	Downcomer Wall and Vessel Lower Head				

Table 3-8 Measurement Items for Core Inlet Temperature Distribution Test

Measurement Item	Sensor Type	Locations	Number
Core Inlet Temperature Distributions	Thermocouples	see Figure 3-12	
Inlet Loop Temperature	Thermocouples	Inlet Loop with Hot Water Injection	
		Normal Inlet Loop	

Table 3-9 Test Matrix with Number Runs and Test Conditions for Hydraulic Test

ID	Structures in Lower Plenum	LCSP Flow Hole Orifice	Loop Flow Rate (percent)	PIV	Inlet Flow Distribution	Pressure Loss	Number of Test Runs (*1)	Test Duration (per Run) (*2)
H1	No Structures	Uniform		X	X	N/A		
H2	Diffuser Plate Assembly	Uniform		X	X	N/A		
H3	Diffuser Plate Assembly	Configured Design		X	X	N/A		
				N/A	X	N/A		
				N/A	N/A	X		

*1 : '+n' means 'n' additional runs to check the repeatability

*2 : Applicable to "Inlet Flow Distribution" and "Pressure Loss"

Table 3-10 Test Matrix with Number Runs and Test Conditions for Flow Induced Vibration

ID	Structures in Lower Plenum	LCSP Flow Hole Orifice	Loop Flow Rate (percent)	Number of Test Runs (*1)	Test Duration (per Run)
F1	Diffuser Plate Assembly	Configured Design			
F2					
F3					
F4					
F5					

*1 : '+n' means 'n' additional runs to check the repeatability

Table 3-11 Test Conditions for Temperature Distribution Measurement

ID	Structures in Lower Plenum	LCSP Flow Hole Orifice	Loop Flow Rate (percent)	Number of Test Runs (*1)	Test Duration (per Run)
T1	Diffuser Plate Assembly	Configured Design	[]

*1 : '+n' means 'n' additional runs to check the repeatability

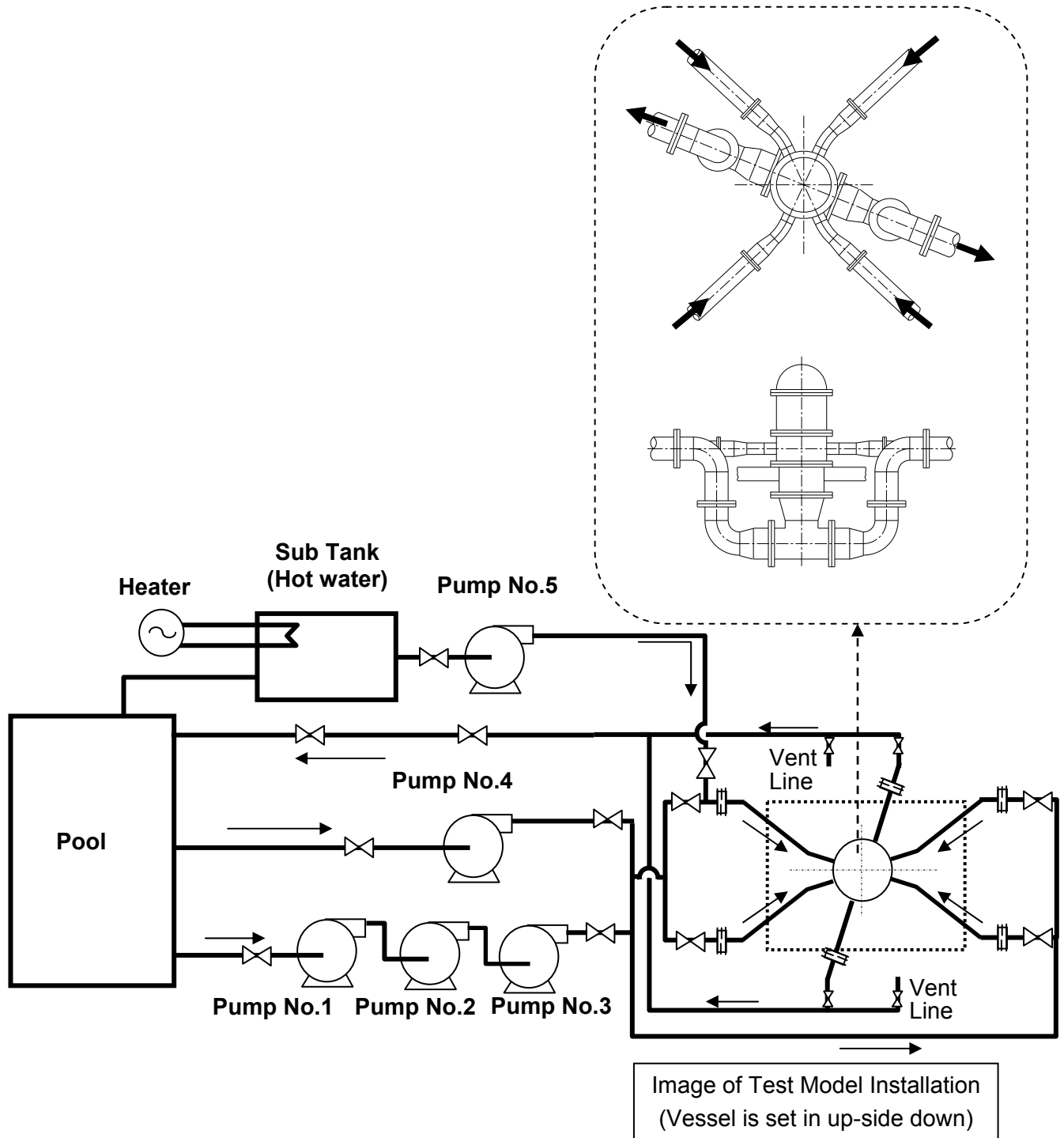


Figure 3-1 Test Loop and Test Model

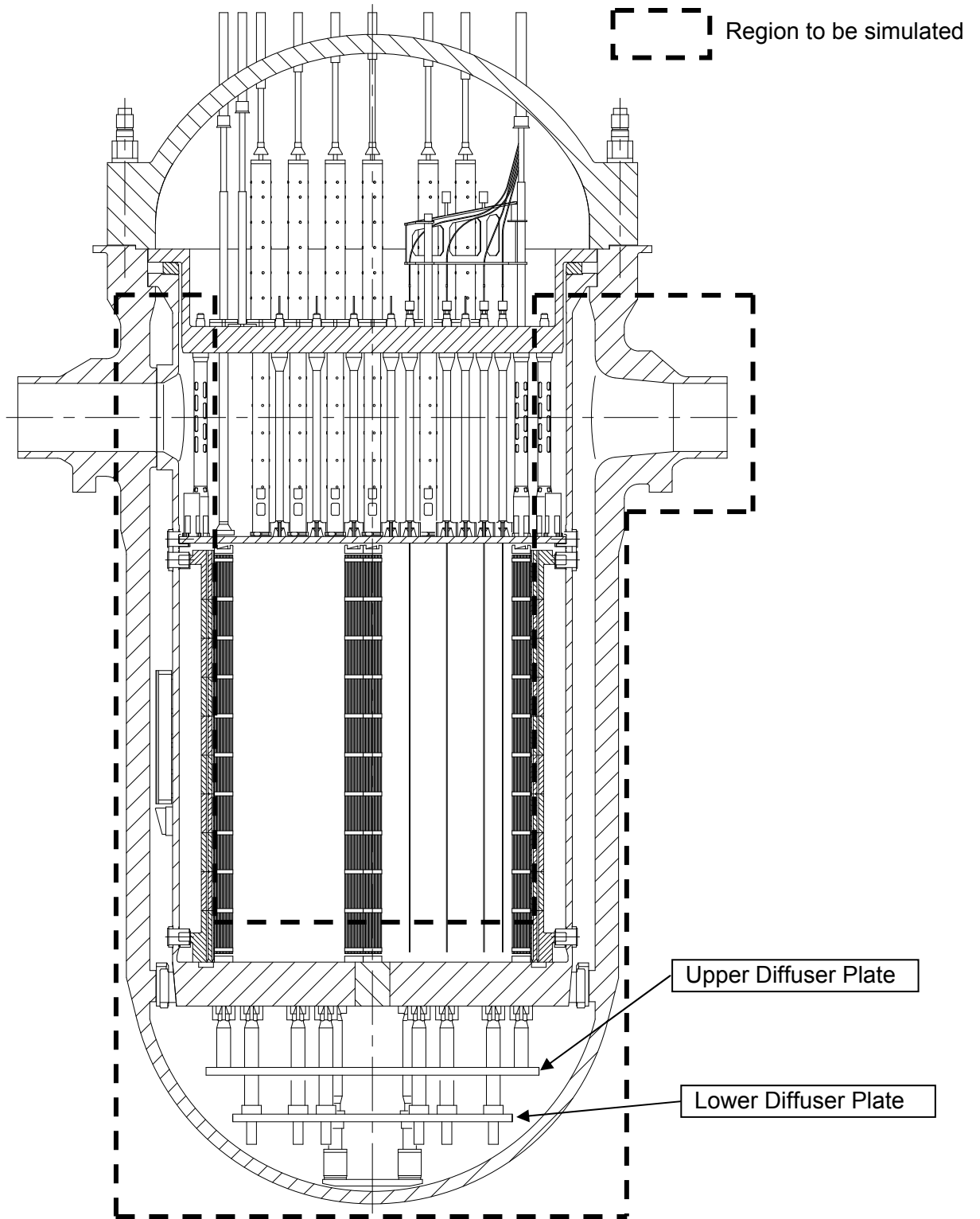


Figure 3-2 Scope of Simulation

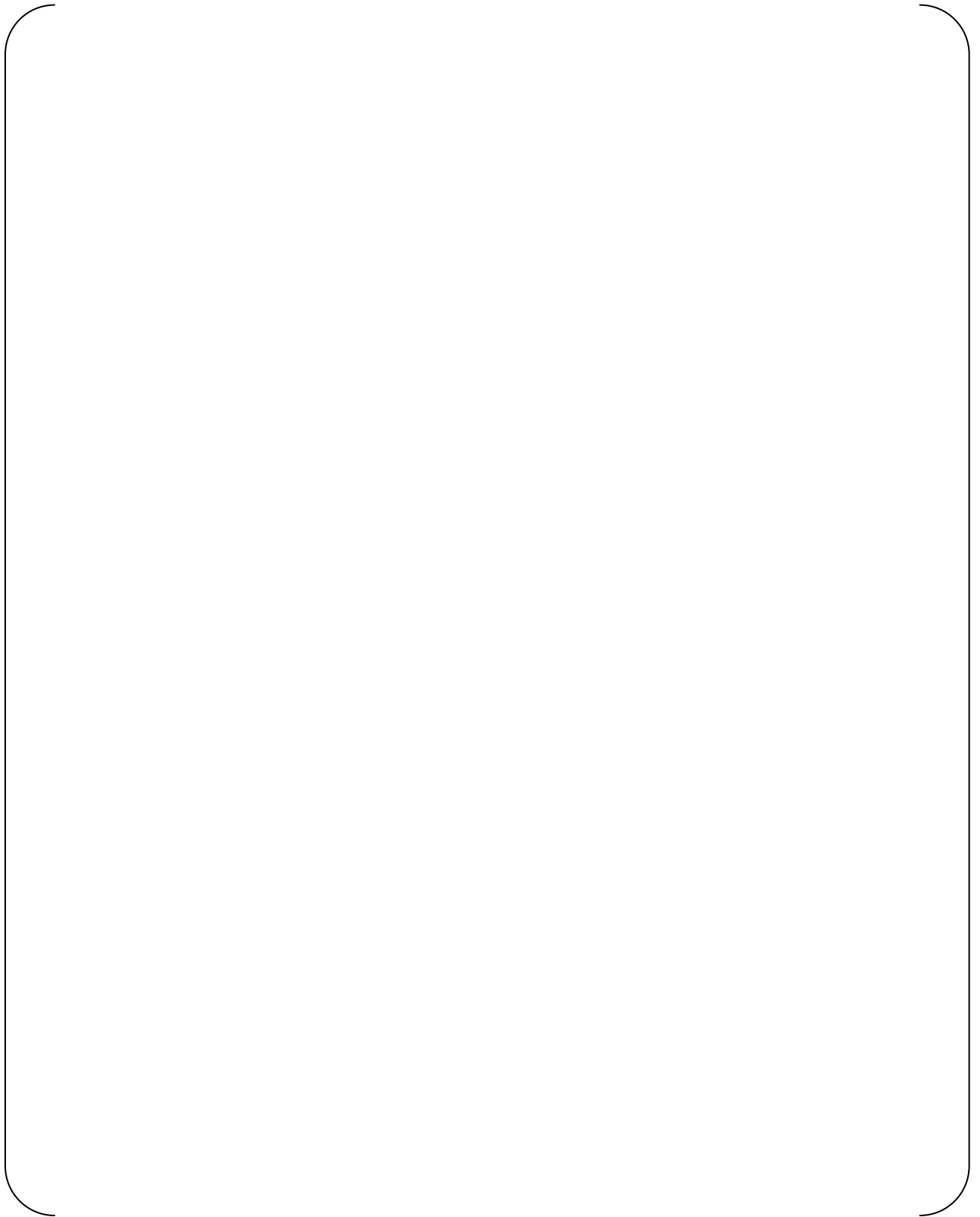


Figure 3-3 Model of Reactor Vessel and Lower Internals (1/7 Scale Model)

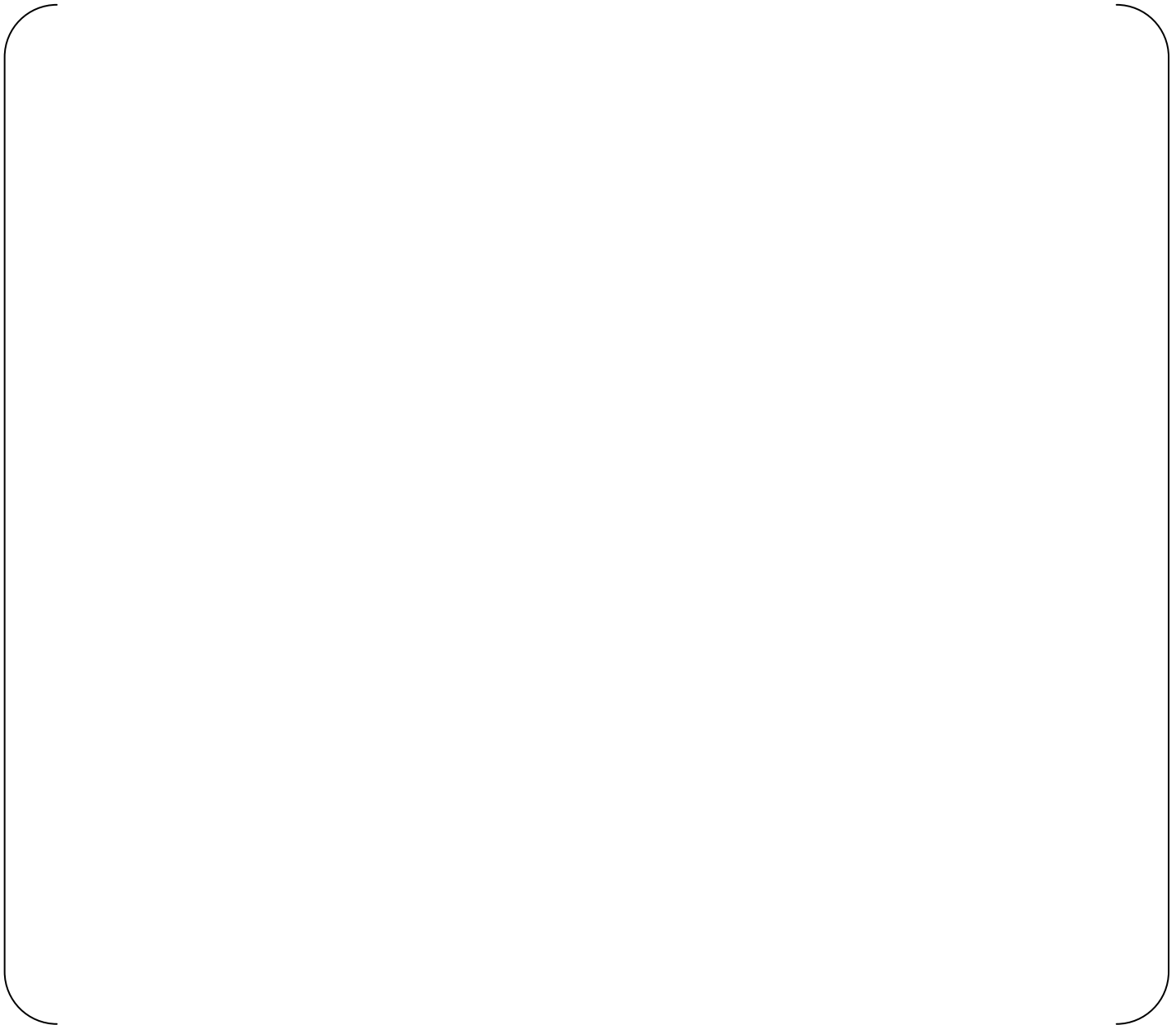


Figure 3-4 Hydraulic Test Measurement Block Diagram

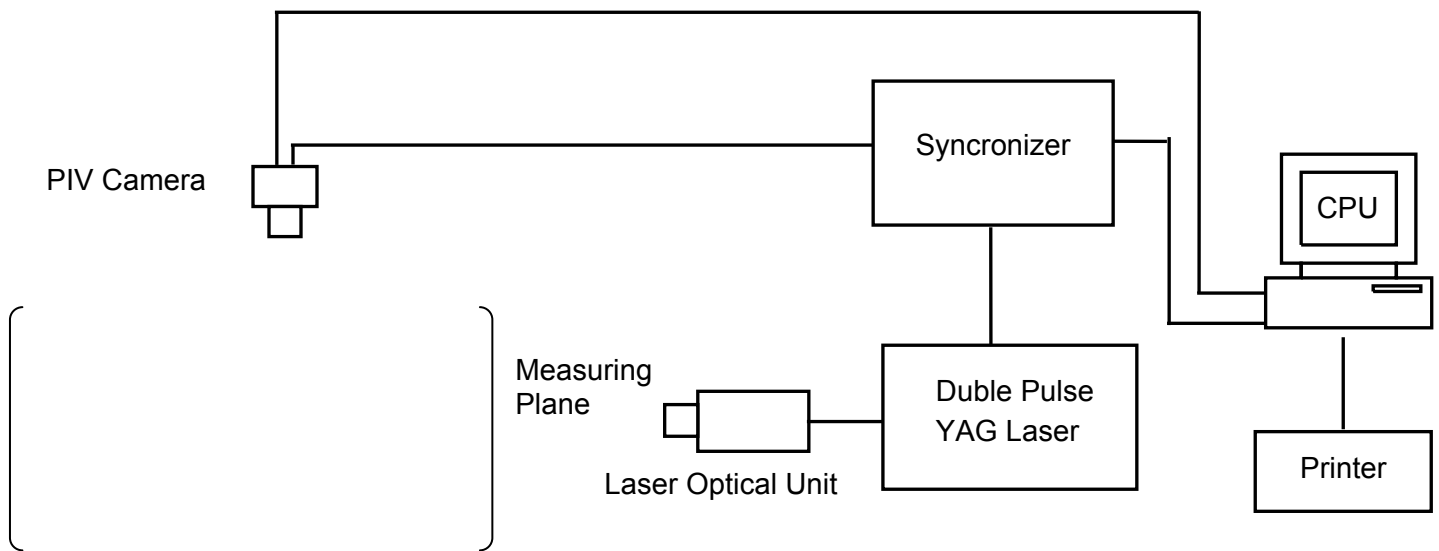


Figure 3-5 PIV System



Figure 3-6 Measuring Locations of Transient History Flow Rate

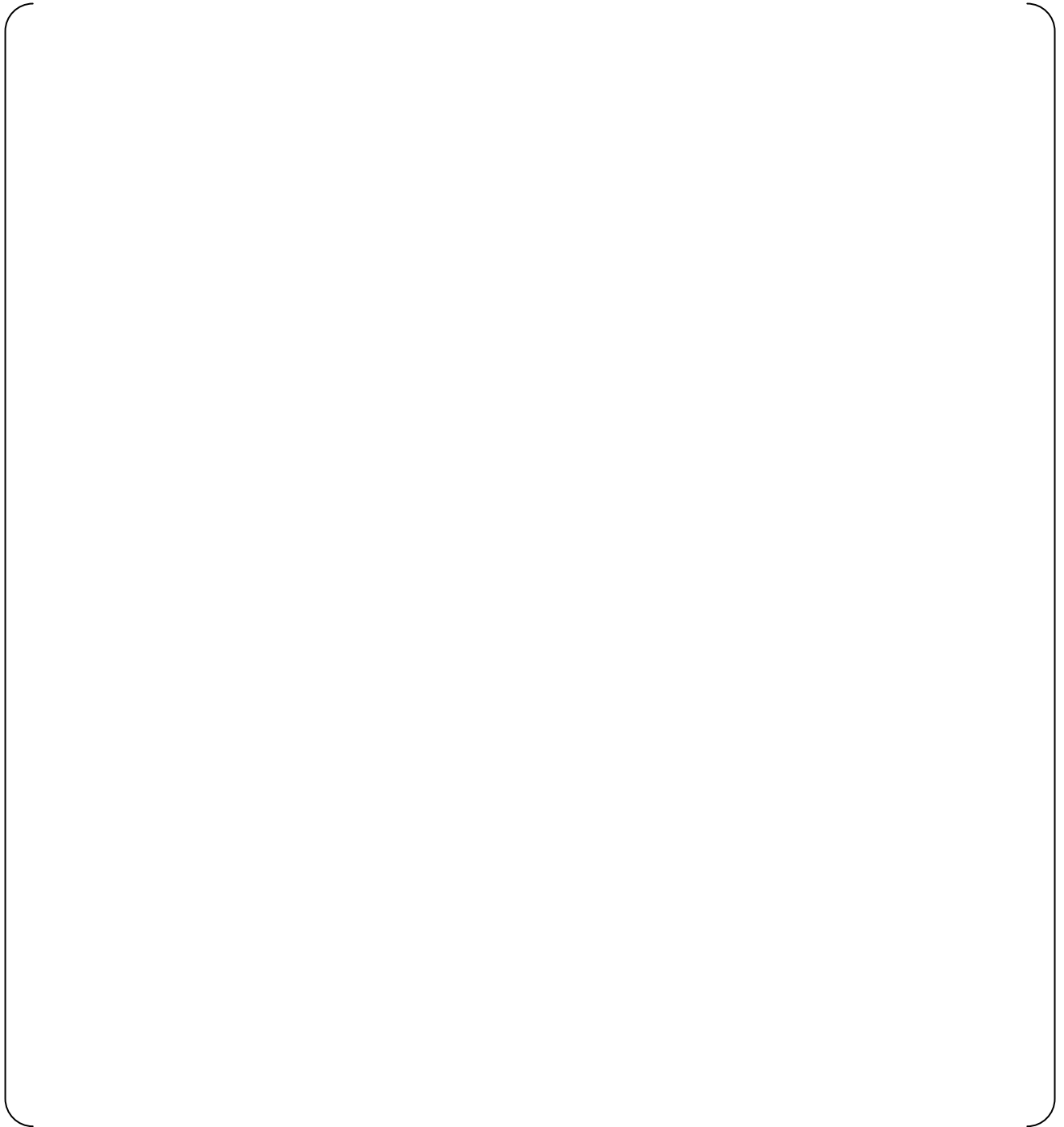


Figure 3-7 Measuring Locations of Inlet Flow Distribution

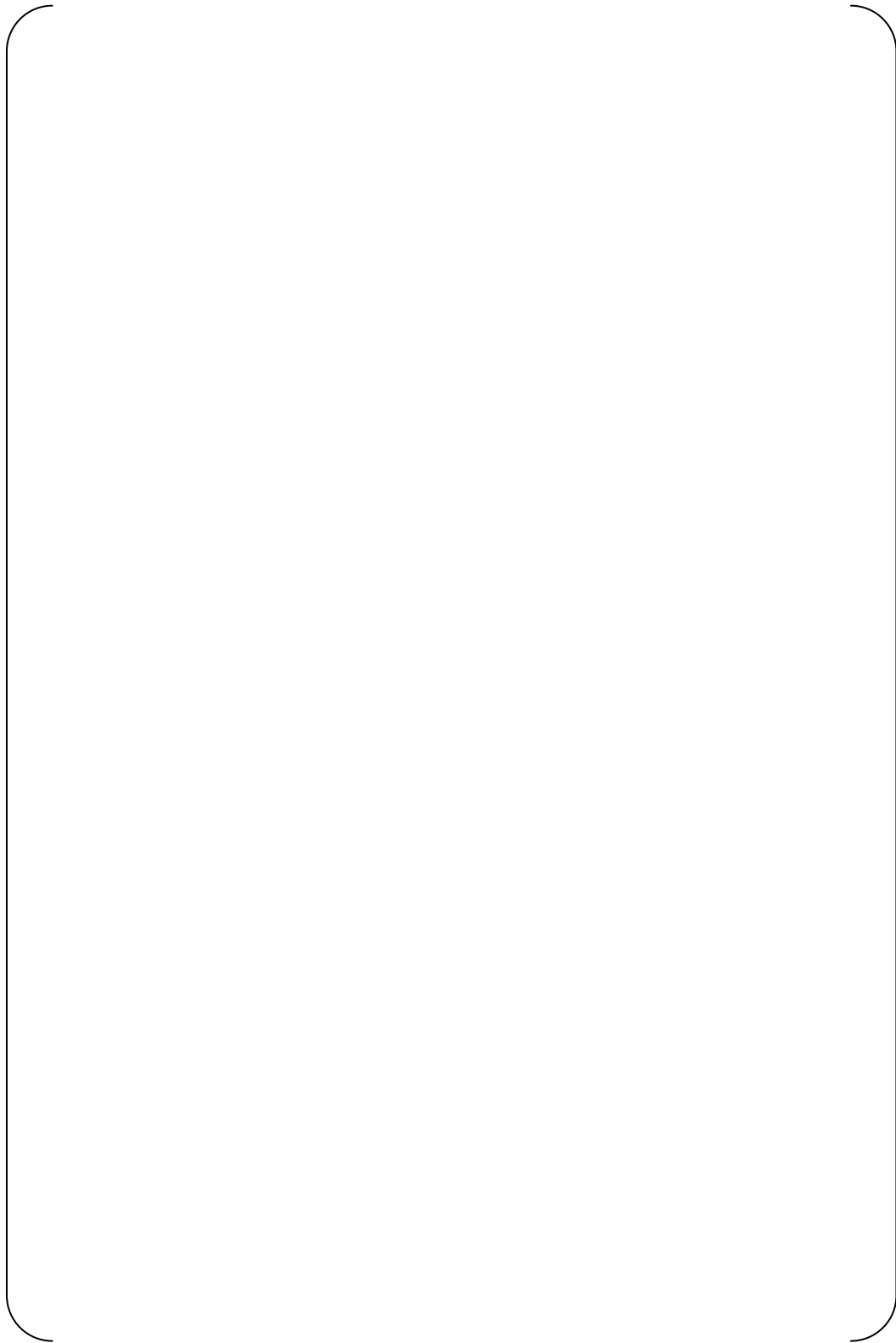


Figure 3-8 Regions for NR Inlet Flow Evaluation

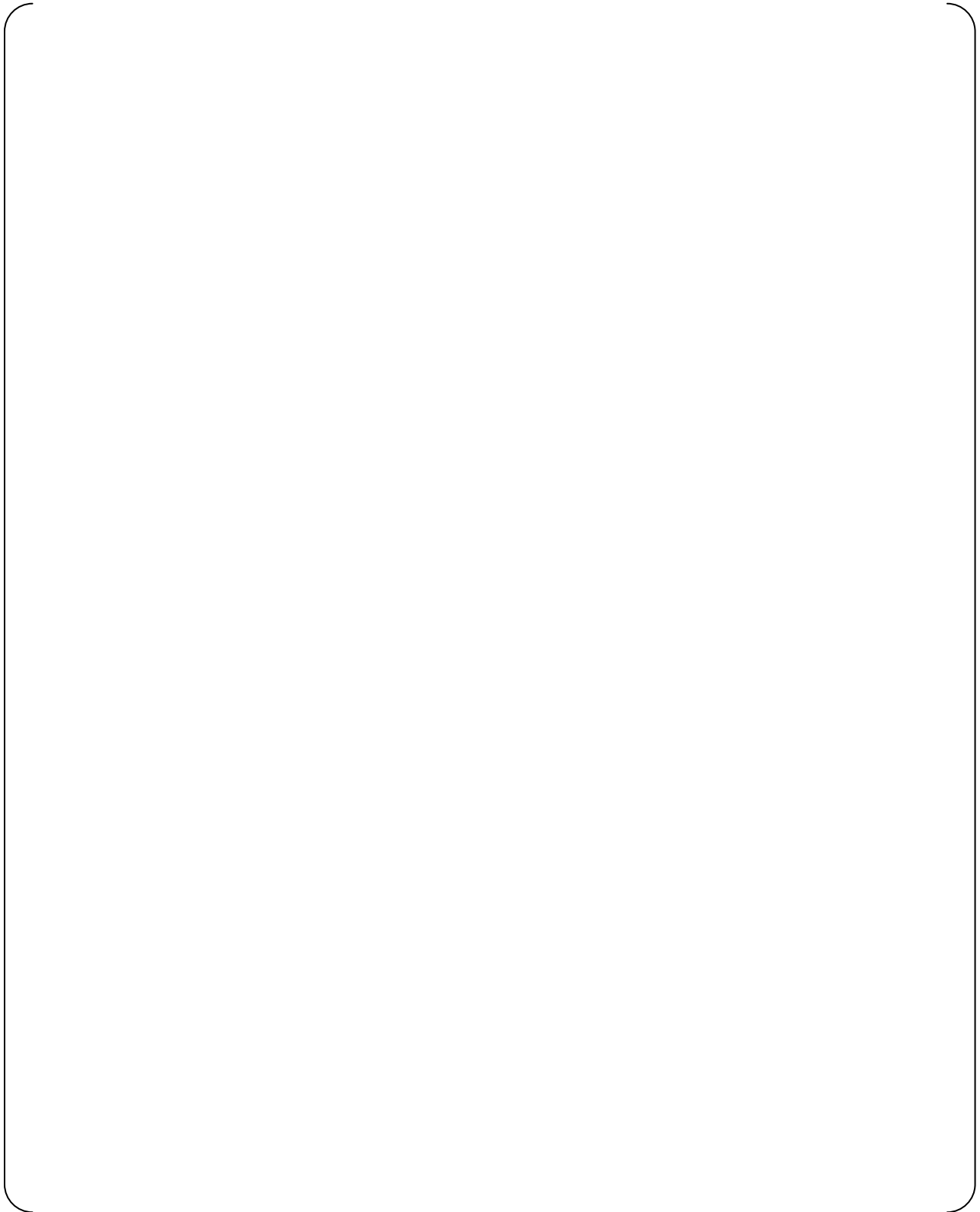


Figure 3-9 Measuring Locations of Pressure



Figure 3-10 Flow-Induced Vibration Measurement Block Diagram

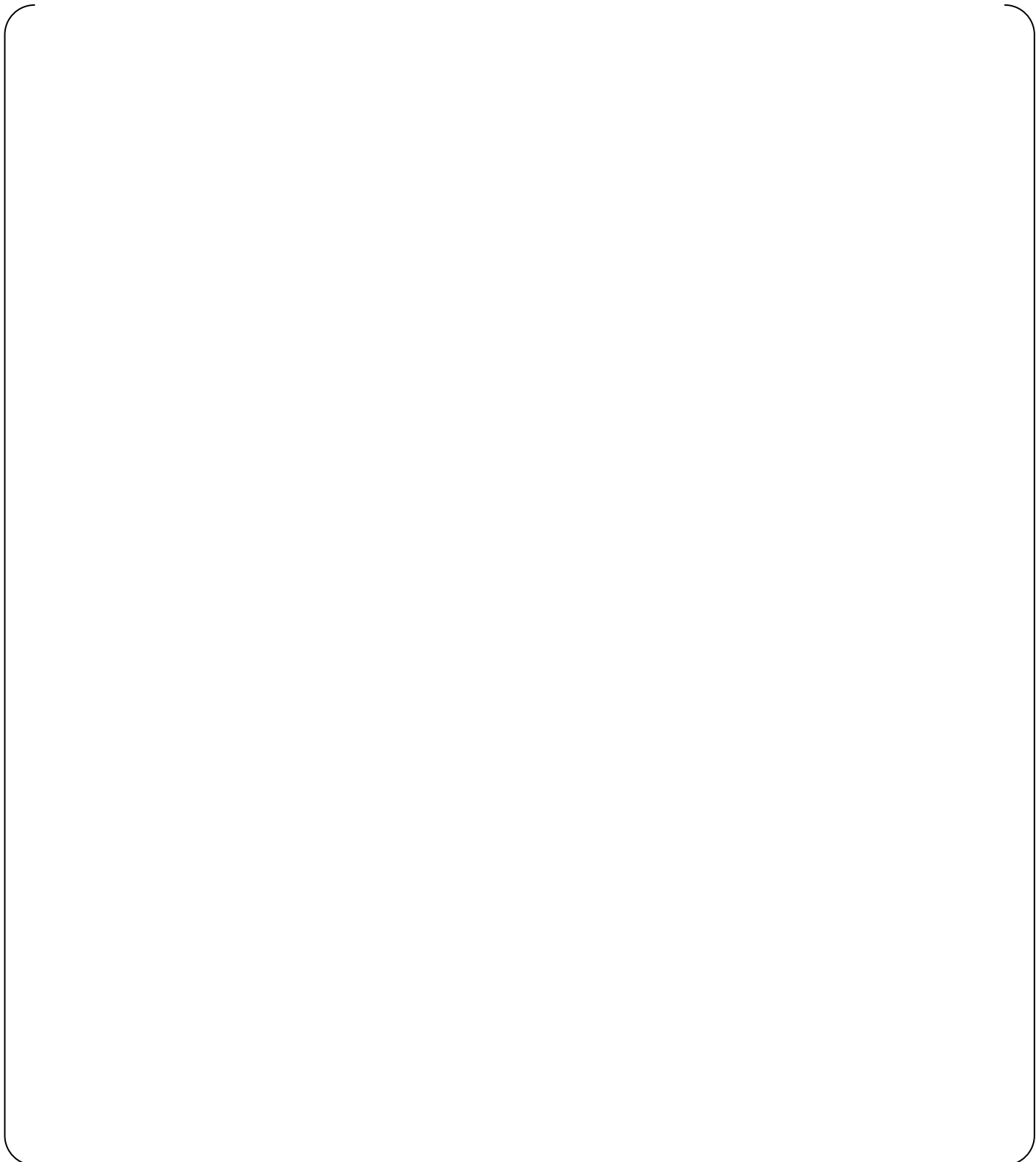


Figure 3-11 Measuring Locations of Flow-Induced Vibrations



Figure 3-12 Measuring Locations of Core Inlet Temperature

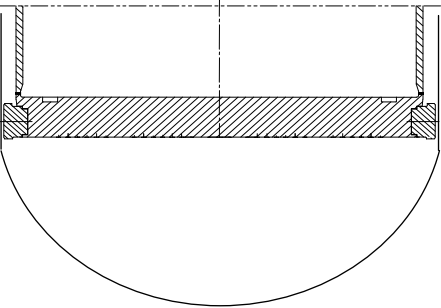
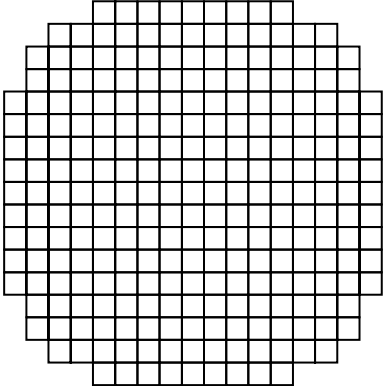
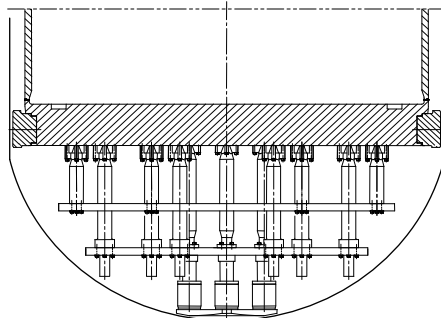
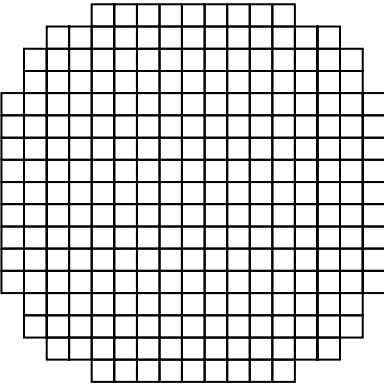
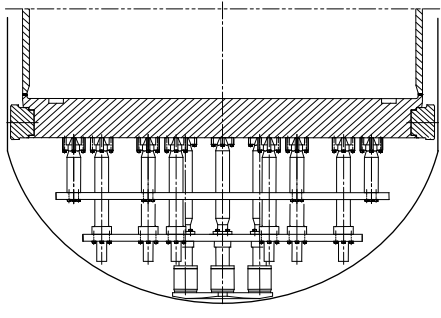

Test ID	Lower Plenum Structure	Flow Hole Orifice Pattern of the Lower Core Support Plate
H1		
H2		
H3 Configured Design		
Remark		

Figure 3-13 Hydraulic Test Configuration

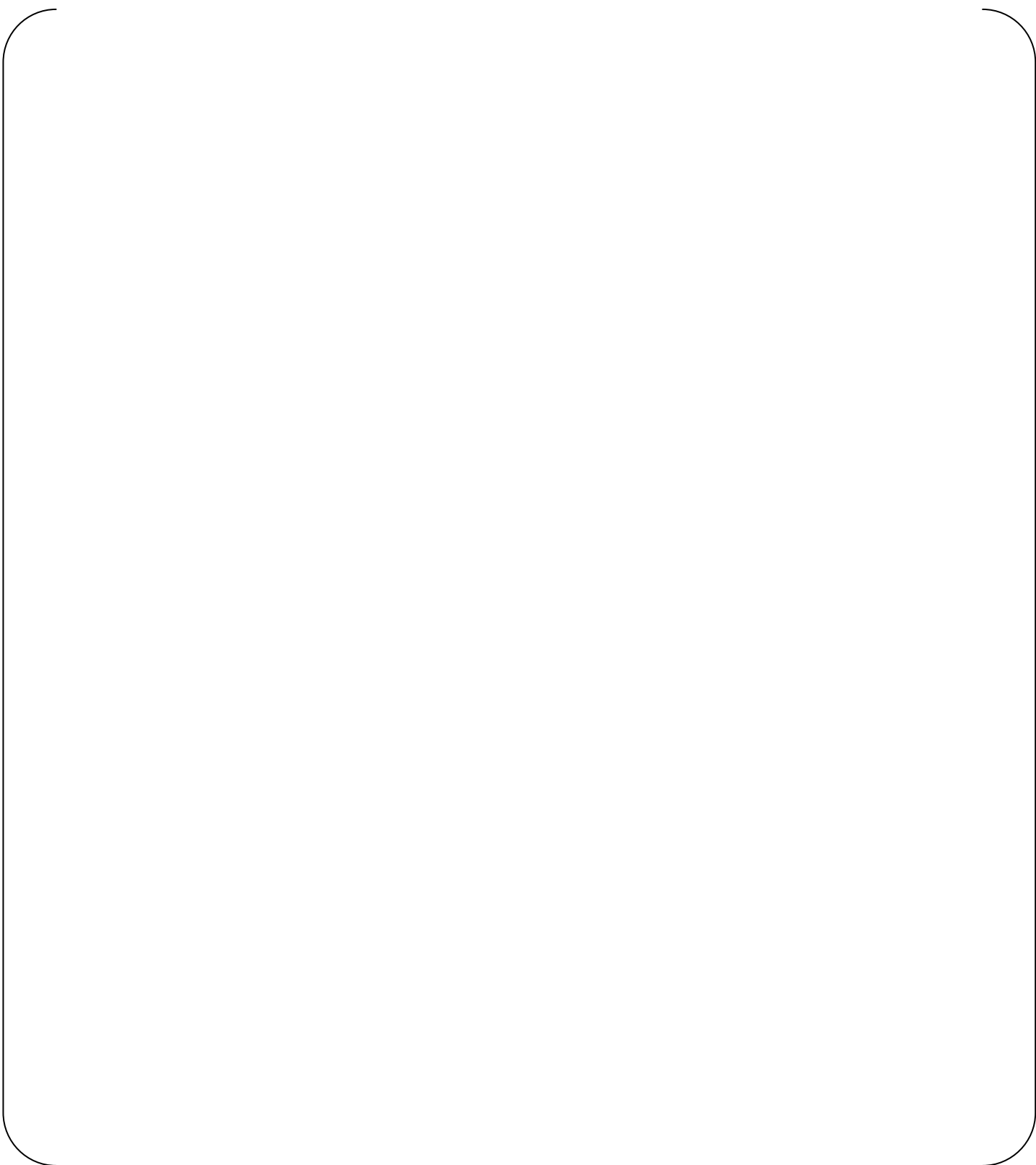


Figure 3-14 Daily Check of Data Repeatability

4. TEST RESULTS AND DISCUSSIONS

4.1 Hydraulic Test

Three steps of tests were performed to evaluate flow stability, core inlet flow distribution, pressure loss and NR inlet flow distribution. These test cases are presented in Table 3-9. Test results were compared with the design targets presented in subsection 1.3.1.

(1) Flow stability

In order to evaluate the flow stability, the velocity field of the lower plenum and the time histories of the core inlet flow rates were measured. The flow velocity distribution was taken in a horizontal plane of the lower plenum and the time histories of the core inlet flow were recorded. The results of these measurements are shown in Figures 4-1 to 4-9. The non-dimensional flow rate is defined by the following equation:

$$\text{Non Dimensional Flow Rate (NDFR)} = \frac{\text{Measured Flow Rate}}{\text{Core Averaged Flow Rate}}$$

a. Test without diffuser plate assembly

The time-averaged velocity field generated from the PIV measurement in Test H1 is shown in Figure 4-1. [

] It can also be observed in Figure 4-2 [

] from the results of core inlet flow rate measurements, as shown in Figure 4-3. [

]

b. Test with diffuser plate assembly

The time-averaged flow velocity fields generated from the PIV measurements in Tests H2 and H3 are shown in Figures 4-4 and 4-7 respectively. These figures clearly show the [

] . It is also observed in Figures 4-5 and 4-8 that [

]

] as shown in Figures 4-6 and 4-9. [

]

Comparing this set of the data with the data from the test without the diffuser plate assembly, the diffuser plate assembly remarkably improves the flow stability. It is concluded that the diffuser plate assembly designed for the US-APWR sufficiently stabilizes the flow in the lower plenum and at core inlet.

(2) Core inlet flow distribution

From the discussions in Subsection 4.1, it was confirmed that the core inlet flow was very much stabilized when the diffuser plate assembly was installed. In evaluating the core inlet flow distribution, the time-averaged core inlet flow rates were used. The core inlet flow distributions were obtained from the measured data at all of the fuel assembly locations. These were presented in Figures 4-10 to 4-14.

a. Test without diffuser plate assembly

The core inlet flow distribution of Test H1, in which the diffuser plate assembly was not installed, is shown in Figure 4-10. [

[] in Figure 4-1 and [] in Figure 4-10 were caused by the []

b. Test with diffuser plate assembly

The core inlet flow distribution of Test H2, in which the diffuser plate assembly was installed, is shown in Figure 4-11. This figure shows that []

[

]

Test H3 was conducted with the diffuser plate assembly and the LCSP with the configured orifices pattern design. The test result is shown in Figure 4-12. This figure shows that []

In the LCSP with configured orifice patten design, [] as shown in Figure 3-13. Tests H2 and H3 were conducted at [

] as shown in Figure 4-13.

Several tapping locations were selected to obtain the vibration mode shapes as shown in Figure 4-16. An accelerometer on each diffuser plate was selected from those shown in Figure 3-10. The selected accelerometers on the diffuser plate assembly are presented in Figure 4-16. In order to obtain the natural frequency of each vibration mode, the acceleration at each location on the diffuser plate was measured after hand tapping by an impact hammer with a load cell. Measurements were conducted both in air and water conditions.

The impact forces were obtained from the load cell at several tapping locations. The transfer functions between the accelerations and the impact forces were derived. The natural frequencies for each subassembly were identified from the peaks of the transfer functions. The vibration mode associated with each natural frequency was obtained from the gain and the phase of the transfer functions.

The natural frequencies and the vibration mode shapes for the upper and lower diffuser plate subassemblies in water are shown in Figure 4-17. The results of the measurements are summarized in Table 4-4.

The natural frequency under plant operating condition was derived considering the scale factor and the temperature difference between the test and under plant operating conditions as discussed in subsection 3.2.2. From the natural frequencies both in air and water, the ratio of the hydrodynamic added mass to the mass of the structure was estimated by the following equation.

$$\frac{M_a}{M_s} = \left(\frac{f_{Tair}}{f_{Twater}} \right)^2 - 1$$

$\frac{M_a}{M_s}$: ratio of the hydrodynamic added mass to the structural mass

f_{Tair}, f_{Twater} : natural frequencies in air and in water under test conditions

The natural frequencies under plant operating condition are derived by considering the scale factor, the difference between the Young's modulus under plant operating and test conditions, and the added mass ratio, by the following equation. In this equation, the added mass ratio was converted from that under the test condition into that under plant operating condition by multiplying the ratio of fluid densities.

$$f_p = f_{Tair} \left(\frac{E_p}{E_T} \right)^{0.5} \left(1 + \frac{M_a \rho_p}{M_s \rho_T} \right)^{-0.5} \frac{1}{7}$$

E_p, E_T : Young's modulus for plant operating and test conditions

ρ_p, ρ_T : fluid density for plant operating and test conditions

f_p : natural frequency for plant operating condition

The natural frequencies under plant operating conditions are shown in Table 4-5. For each subassembly, the lowest natural frequency was selected from those shown in Table 4-5 to assess the potential for fluid-elastic instability. The selected lowest frequency was used in the evaluation of vortex shedding lock-in because the estimated vortex shedding frequency was

lower than the lowest natural frequency. The selected frequencies were [] Hz for the lower diffuser plate subassembly and [] Hz for the upper diffuser plate subassembly.

The critical flow velocity for fluid-elastic instability was derived following the Conner's equation, which was presented in the FIV guideline in ASME Sec. III (Ref.7).

$$\frac{U_c}{f_n D} = C \left(\frac{m \delta}{\rho D^2} \right)^\alpha$$

- U_c : critical gap flow velocity for fluid elastic instability (in/s)
 f_n : lowest natural frequency of diffuser plate subassembly (Hz)
 D : diameter of diffuser support column (in)
 m : mass of diffuser plate subassembly divided by the length of the diffuser support column. It includes the hydraulic added mass (lb·s²/in²)
 δ : logarithmic decrement of the diffuser plate subassembly, $\delta = [\quad]$ was applied according to the Regulatory Guide 1.20.
 ρ : fluid density (lb·s²/in⁴)
 C, α : coefficients for critical flow velocity. C=2.4 and $\alpha = 0.5$ were applied according to the suggested numbers in FIG. N-1331-4 of Reference 7

The gap velocity between the diffuser plate support columns was conservatively calculated using the following equation based on the flow velocity in the downcomer.

$$U = \frac{P U_0}{P - D}$$

- U : gap flow velocity between diffuser support columns
 U_0 : flow velocity in the downcomer
 P : pitch of diffuser support columns

The margin of safety for fluid-elastic instability of the diffuser plate subassembly was evaluated with the following equation.

$$M.S. = \frac{U_c}{U} - 1$$

- $M.S.$: margin of safety for fluid elastic vibration

The design guidelines for avoiding of vortex shedding lock-in are suggested in N1324 of Reference 7. It is required that at least one of the following three conditions must be satisfied to avoid vortex shedding lock-in.

$$\frac{U}{f_n D} < 1.0,$$

$$\frac{U}{f_n D} < 3.3 \quad \text{and} \quad \frac{m\delta}{\rho D^2} > 1.2$$

$$f_n < 0.7f_s \quad \text{or} \quad f_n > 1.3f_s$$

,where f_s is vortex shedding frequency, given by the following equation.

$$f_s = S_t \frac{U}{D}$$

Where the Strouhal number S_t was determined to be [] from the FIG. N-1331-4 of Reference 7.

The computed margins of safety against fluid-elastic instability are presented in Table 4-6. The natural frequencies were sufficiently high to avoid fluid-elastic instability. The gap velocity was less than the critical velocity. Consequently, the margin of safety was positive. It is concluded that fluid-elastic instability will not occur.

The computed parameters for the evaluation of vortex shedding lock-in are presented in Table 4-7. The natural frequencies were more than thirty percent higher than the vortex shedding frequency. It is concluded that the lock-in will not occur.

(2) Flow-Induced Vibration Response

Flow-induced vibration tests were performed at five flow conditions. To confirm the absence of the abnormal vibrations and high cycle fatigue, time histories of strains on the diffuser support columns were measured as shown in Figure 3-10. The test cases are presented in Table 3-10. The test results are compared with the design targets presented in subsection 1.3.2.

a. Absence of abnormal vibrations

From the time histories of strain data, the root mean square (rms) vibration responses were derived under each flow rate condition. The relationships between the rms responses and the flow rates are shown in Figure 4-18. In this figure, the measured rms numbers are compared with the proportionality line to the square of the flow rate. As shown in this figure, the vibration responses show good agreements with the slope of the proportionality lines. The measured data does not show sudden changes under any flow conditions.

Based on the test results and analytical studies discussed in subsection 4.1 (1) b, it is concluded that the abnormal vibrations such as the fluid-elastic vibration or vortex shedding lock-in did not occur.

b. High cycle fatigue

High cycle fatigue evaluations of the structures in the lower plenum were performed based on the method discussed in subsection 3.4.2.

The amplitudes of alternating stresses in the test model were derived by multiplying the measured rms strains with the ratio of peak to rms amplitudes (peak factor) and the Young's

modulus at the test temperature. This amplitude at the measurement point was translated into the amplitude of peak stress under plant conditions by adjusting for the differences in the fluid mass densities, the section moduli, the stress concentration factors and the ratio of Young's moduli at the test and at the actual plant operating temperatures. The amplitudes of alternating stress intensity were derived from the following equation.

$$S = \varepsilon_{rms} \times K_{rms} \times E_T \times \frac{\rho_P}{\rho_T} \times \frac{Z'}{Z} \times K_{ST} \times \frac{E_T}{E_P} < S_a$$

S : amplitude of the alternating stress intensity (ksi)

ε_{rms} : rms amplitude of the measured strain

K_{rms} : assumed ratio of peak amplitude to rms response ; [] (peak factor)

E_T : Young's modulus of the austenitic stainless steel at the room temperature ; 28.3×10^3 ksi (Ref.2)

ρ_P / ρ_T : ratio of fluid densities under plant operating condition and at the room temperature

Z'/Z : ratio of section moduli at the measurement point to the stress evaluation point as shown in Table 4-8

K_{ST} : stress concentration factor for discontinuous structures ; 5 (Ref.8)

E_P : Young's modulus of the austenitic stainless steel under plant operating condition [] ksi (Ref.9)

S_a : allowable amplitude of alternating stress intensities for 10^{11} cycles based on the ASME design fatigue curve; 13.6 ksi (Ref.2)

The amplitudes of the alternating stress intensity are presented in Table 4-9. It was confirmed that the maximum amplitude was [] ksi. This number is smaller than the limit for 10^{11} cycles in the ASME design fatigue curve in Reference 2.

From the test results mentioned above, it was concluded that the diffuser plate assembly of the US-APWR satisfied the design criterion for high cycle fatigue.

4.3 Core Inlet Temperature Distribution Test

The core inlet temperature distribution test under asymmetric loop cooling condition was performed to confirm that adopted core inlet temperature distribution model for the safety analysis was adequate for the core inlet temperature distribution. The test condition is presented in Table 3-11. In the test, hot water was provided from the event loop instead of the cold water in the safety analysis.

In order to evaluate the core inlet temperature distribution, the time-averaged coolant temperatures were measured at the locations in Figure 3-12. The core inlet temperature is converted into the non-dimensional temperature defined in the following:

$$f_i = \frac{T_{local}^i - T_{normal}}{T_{event} - T_{normal}}$$

- f_i : non-dimensional temperature at i -th location in the core
 T_{local}^i : local temperature at i -th location in the core
 T_{event} : temperature in the event loop (hot water loop in the test)
 T_{normal} : temperature in the normal loop (cold water loop in the test)

The distribution of the non-dimensional temperature is shown in Figure 4-19. The hot water injected from one of the loops was mixed with cold water from the other loops in the downcomer and in the lower plenum. However, the mixing is incomplete, therefore, some considerable temperature distribution remains at the core inlet.

Since the core inlet temperature distribution is also taken into the consideration in the safety analysis of asymmetric cooling events such as Steam System Piping Failure, the test results were compared with the condition in the safety analysis.

In the safety analysis model (Ref.10), [] as shown in Figure 4-20. []
 These values were compared with those used in the safety analysis model for the US-APWR in Figure 4-21. []

The test results indicated that the mixing effect was better than that assumed in the safety analysis model. []

A sensitivity study for the typical Steam System Piping Failure analysis for the US-APWR was performed, in order to estimate the impact on the safety analysis. A small increase of Min. DNBR [] was shown in the sensitivity analysis that adopted the test result as shown in Figure 4-21.

Based on the above discussions, it is concluded that the safety analysis model used for the US-APWR provides the conservative inlet temperature distribution for the asymmetric loop cooling events and it does not have a significant effect on the safety analysis result.

Table 4-1 Results of Core Inlet Flow Distributions (Test H3)

Item	Flow Condition	Test Result	Design Target Values
Minimum Assembly Flow			
Maximum Assembly Flow			
Difference between Adjacent Assemblies			

Table 4-2 Comparison of Core Inlet Flow Distribution between All Loop Operation and N-1 Loop Operation

	Max. Flow Rate	Min. Flow Rate	Flow Rates in Quadrants of Core			
All Loop Operation						
N-1 Loop Operation						

[]

Table 4-3 NR Inlet Flow Rate Distribution

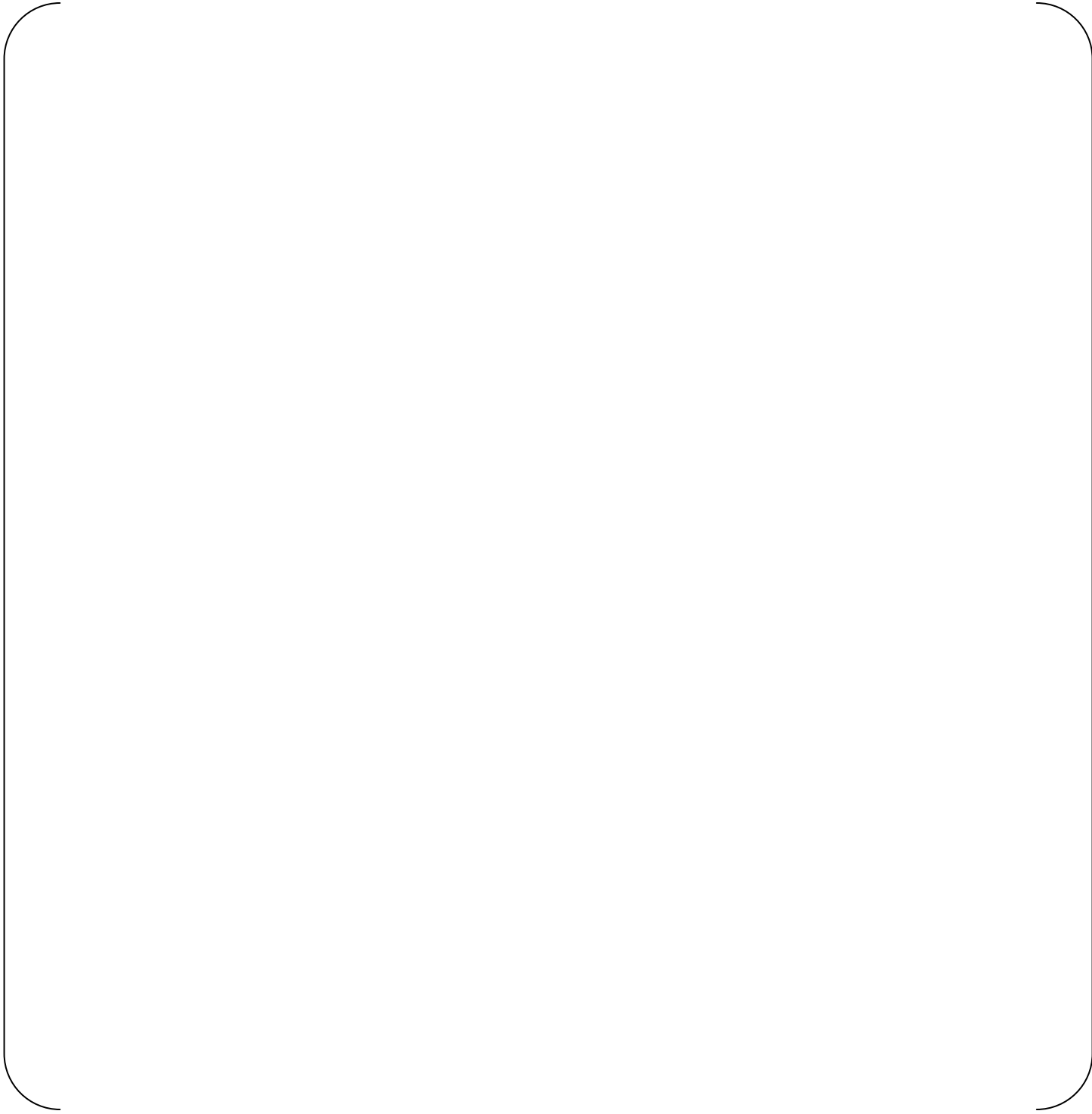


Table 4-4 Natural Frequencies of Diffuser Plate Subassembly

	Vibration Mode	Test Results (Hz)	
		In Air	In Water
Upper Diffuser Plate Subassembly			
Lower Diffuser Plate Subassembly			

Table 4-5 Natural Frequencies under Plant Operating Conditions

	Vibration Mode	Natural frequency (Hz)
Upper Diffuser Plate Subassembly		
Lower Diffuser Plate Subassembly		

Table 4-6 Margins of Safety for Fluid-Elastic Instability

	U (in/s)	D (in)	f_n (Hz)	$U / f_n D$	$m\delta/\rho D^2$	U_c (in/s)	M.S.
Lower Diffuser Plate Subassembly							
Upper Diffuser Plate Subassembly							

Table 4-7 Evaluation for Vortex Shedding Lock-in

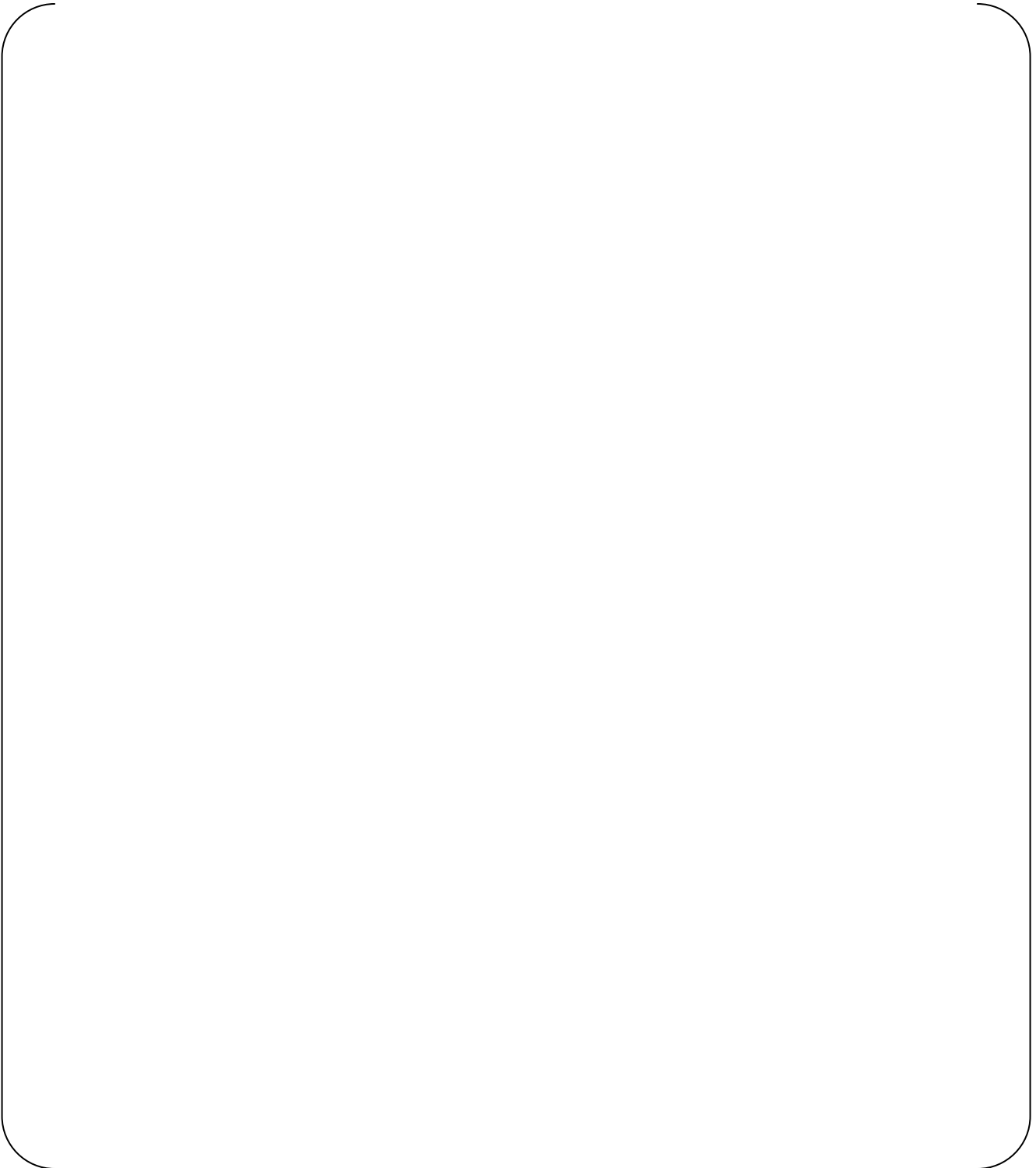
ASME Design Guidelines	N1324(a)	N1324(b)	N1324(d)	Evaluation
	$U/f_n D < 1.0$	$U/f_n D < 3.3$ and $m\delta/\rho D^2 > 1.2$	$f_n < 0.7f_s$ or $f_n > 1.3f_s$	
Lower Diffuser Plate Subassembly				Lock-in is not Occurred
Upper Diffuser Plate Subassembly				Lock-in is not Occurred

Table 4-8 Section Modulus Ratio of Measurement Points and Evaluation Point

Measurement Parts	Measurement Section and Evaluation Section	Section Modulus Ratio (Measuring/Evaluation)
Upper Support Column		
Lower Support Column		
Column Extension		
Secondary Core Support Column		

Table 4-9 Results of High Cycle Fatigue Evaluation

Measurement Parts	Sensor Location	rms of Measured Strain ($\times 10^{-6}$)	Amplitude of Alternating Stress Intensity(ksi)	Allowable Alternating Stress Intensity(ksi)
Upper Diffuser Plate Support Column (LCSP Side)				13.6
Lower Diffuser Plate Support Column (LCSP Side)				
Secondary Core Support Column (LCSP Side)				
Column Extension				



**Figure 4-1 Time-Averaged Velocity Map by PIV (without Diffuser Plate Assembly:
Test H1)**



Figure 4-2 Snap-Shots of Velocity Map by PIV (without Diffuser Plate Assembly: Test H1)

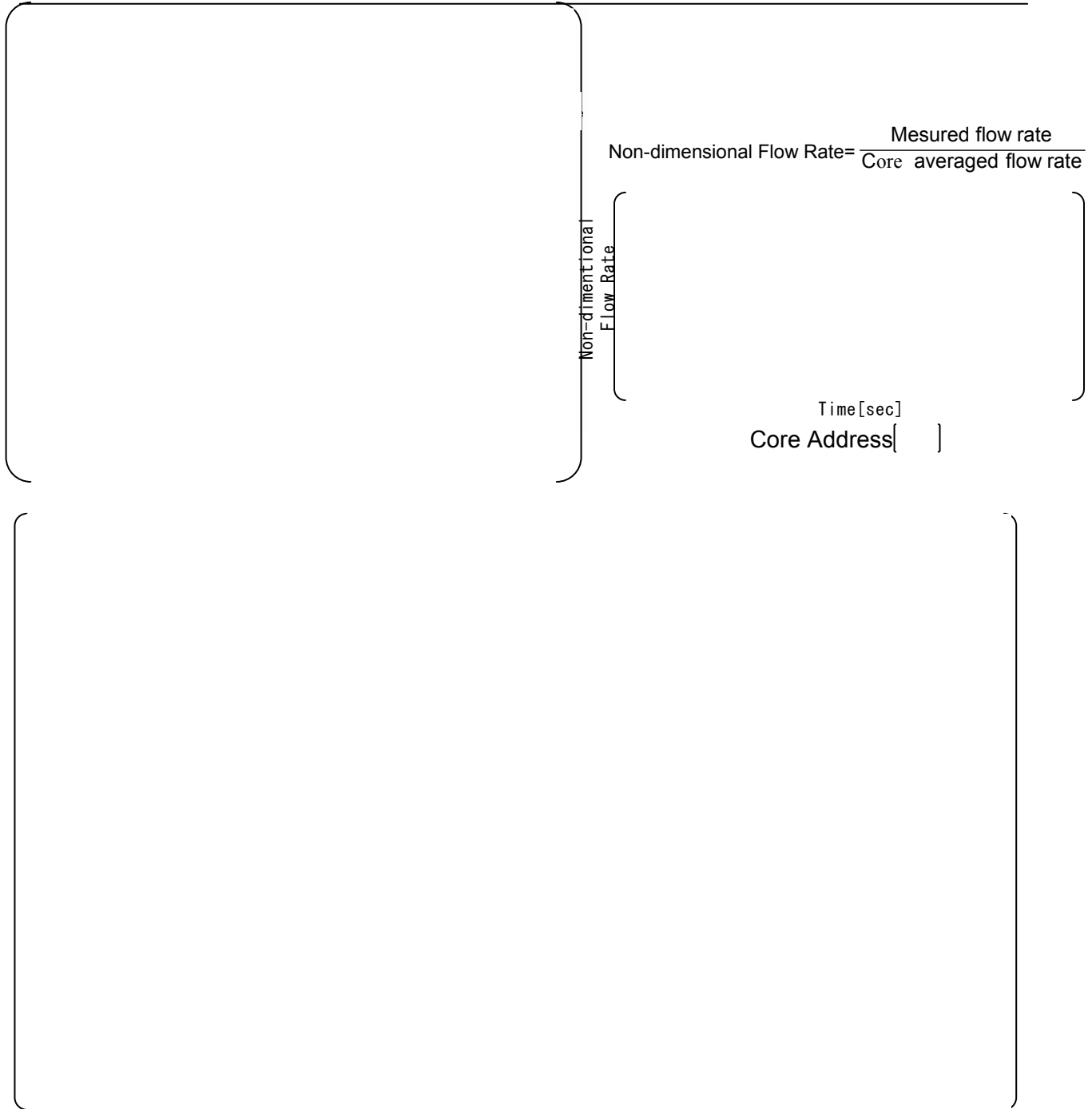


Figure 4-3 Time History of Flow Rate Distribution (without Diffuser Plate Assembly: Test H1)

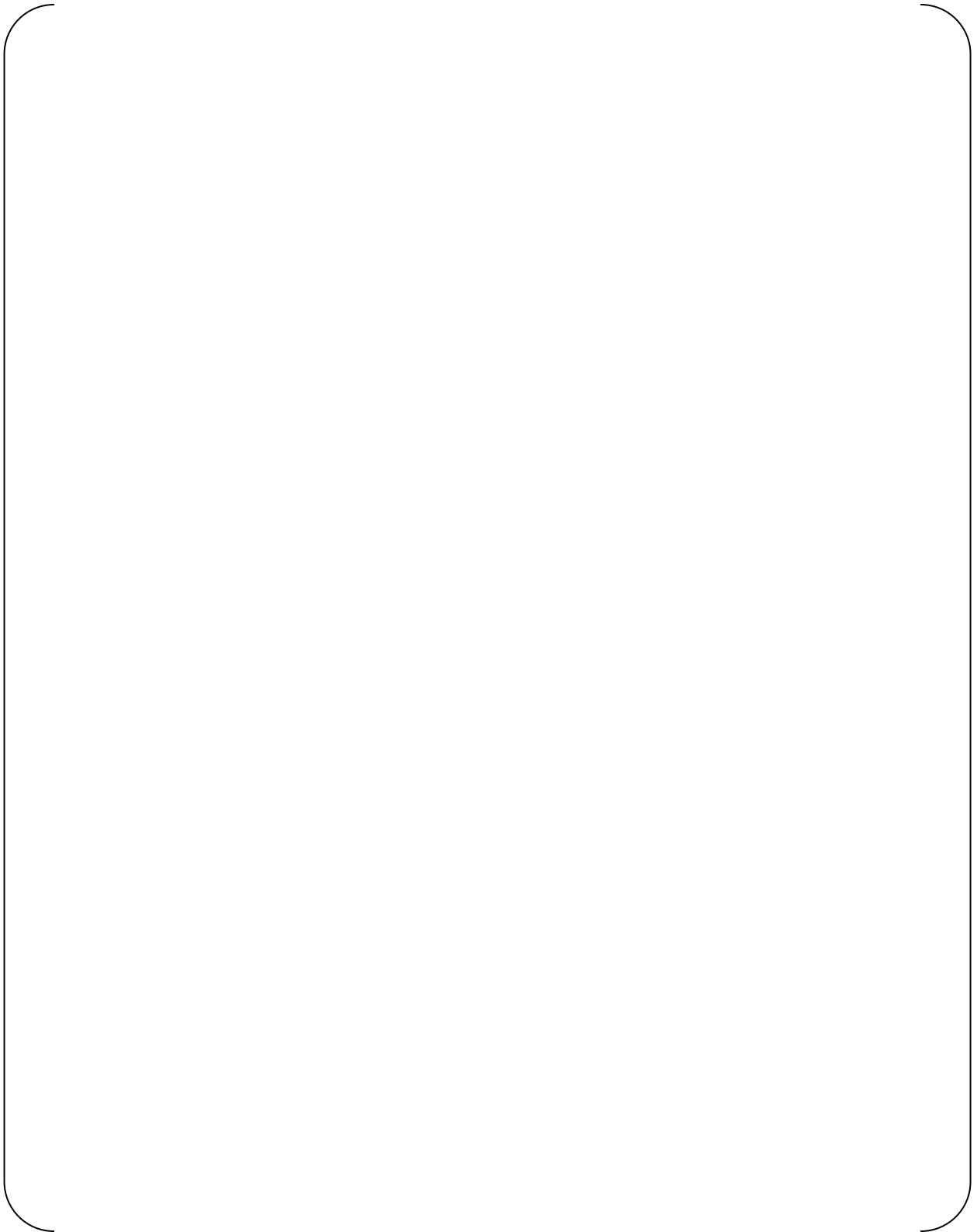


Figure 4-4 Time-Averaged Velocity Map by PIV (with Diffuser Plate Assembly: Test H2)

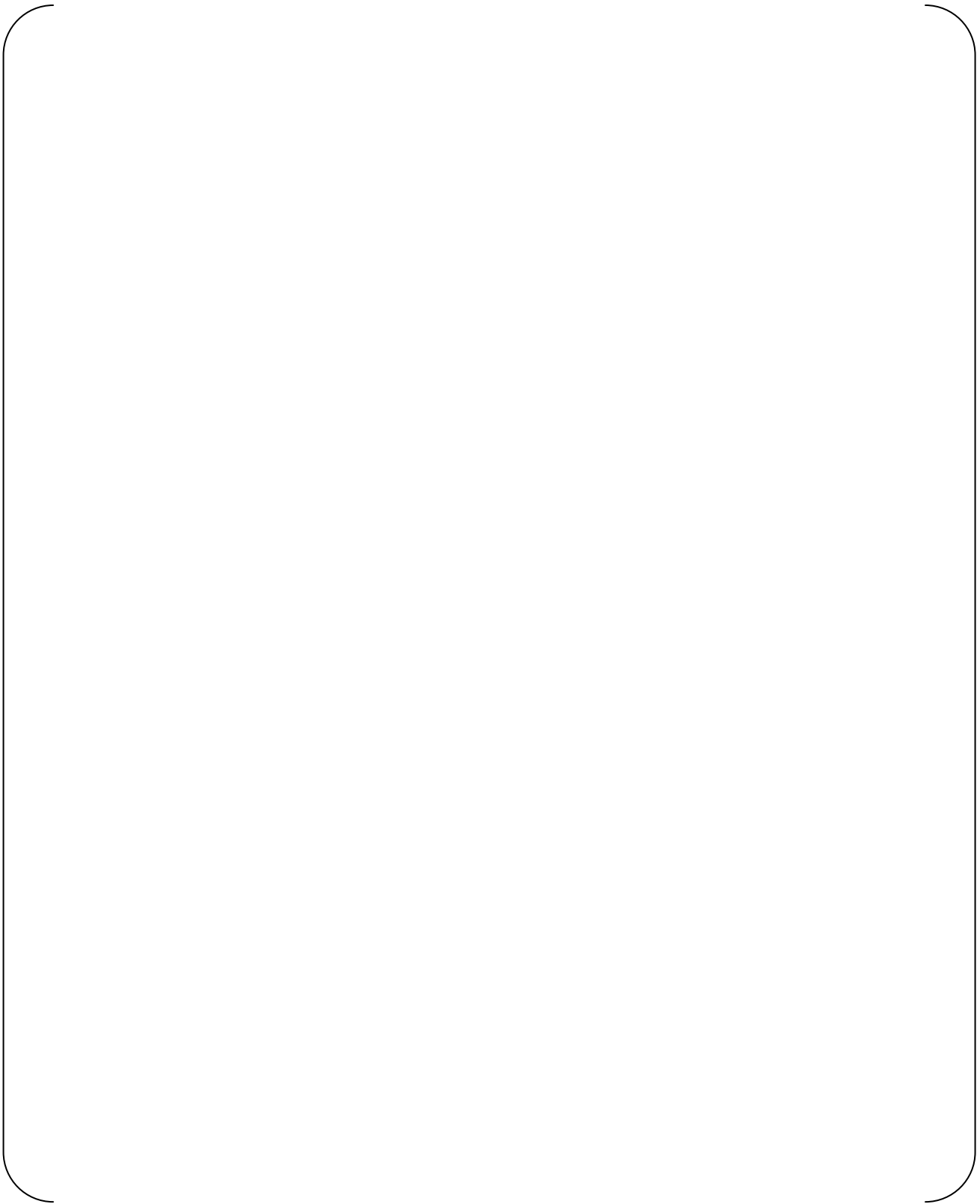


Figure 4-5 Snap-Shots of Velocity Map by PIV (with Diffuser Plate Assembly: Test H2)

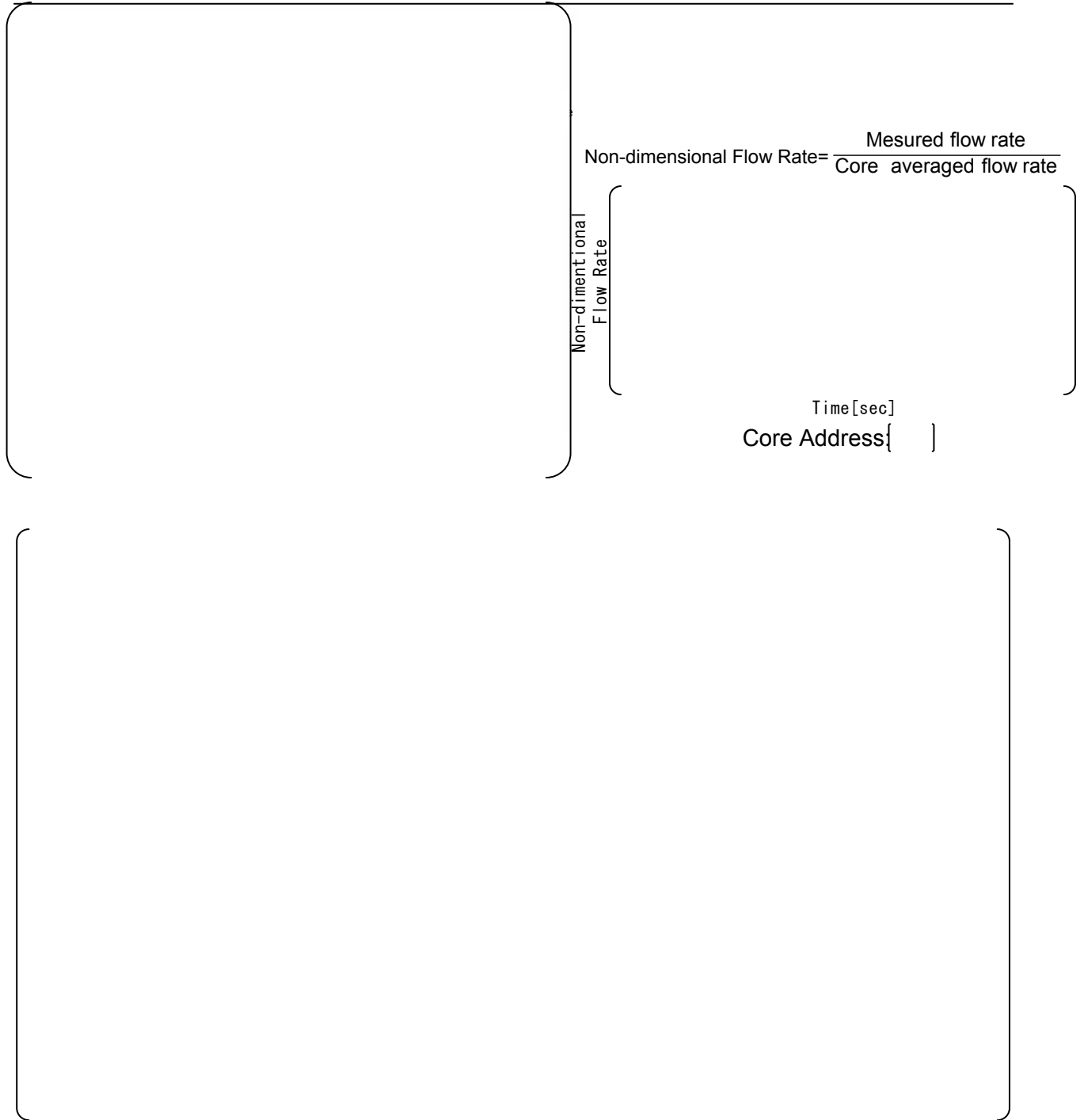


Figure 4-6 Time History of Flow Rate Distribution(with Diffuser Plate Assembly: Test H2)

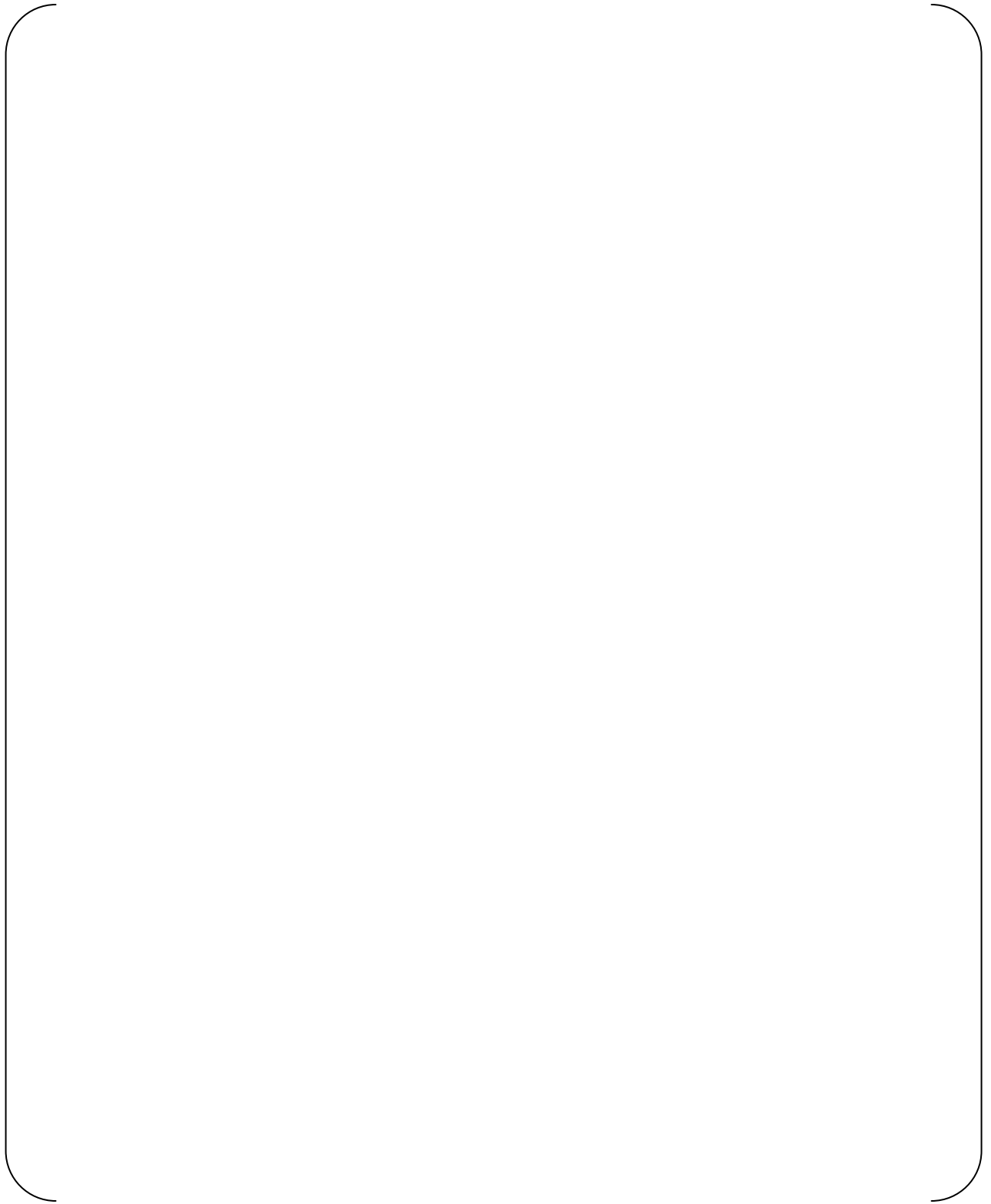


Figure 4-7 Time-Averaged Velocity Map by PIV(with Diffuser Plate Assembly and Design LCSP Flow Hole Pattern: Test H3)



Figure 4-8 Snap-Shots of Velocity Map by PIV(with Diffuser Plate Assembly and Design LCSP Flow Hole Pattern: Test H3)

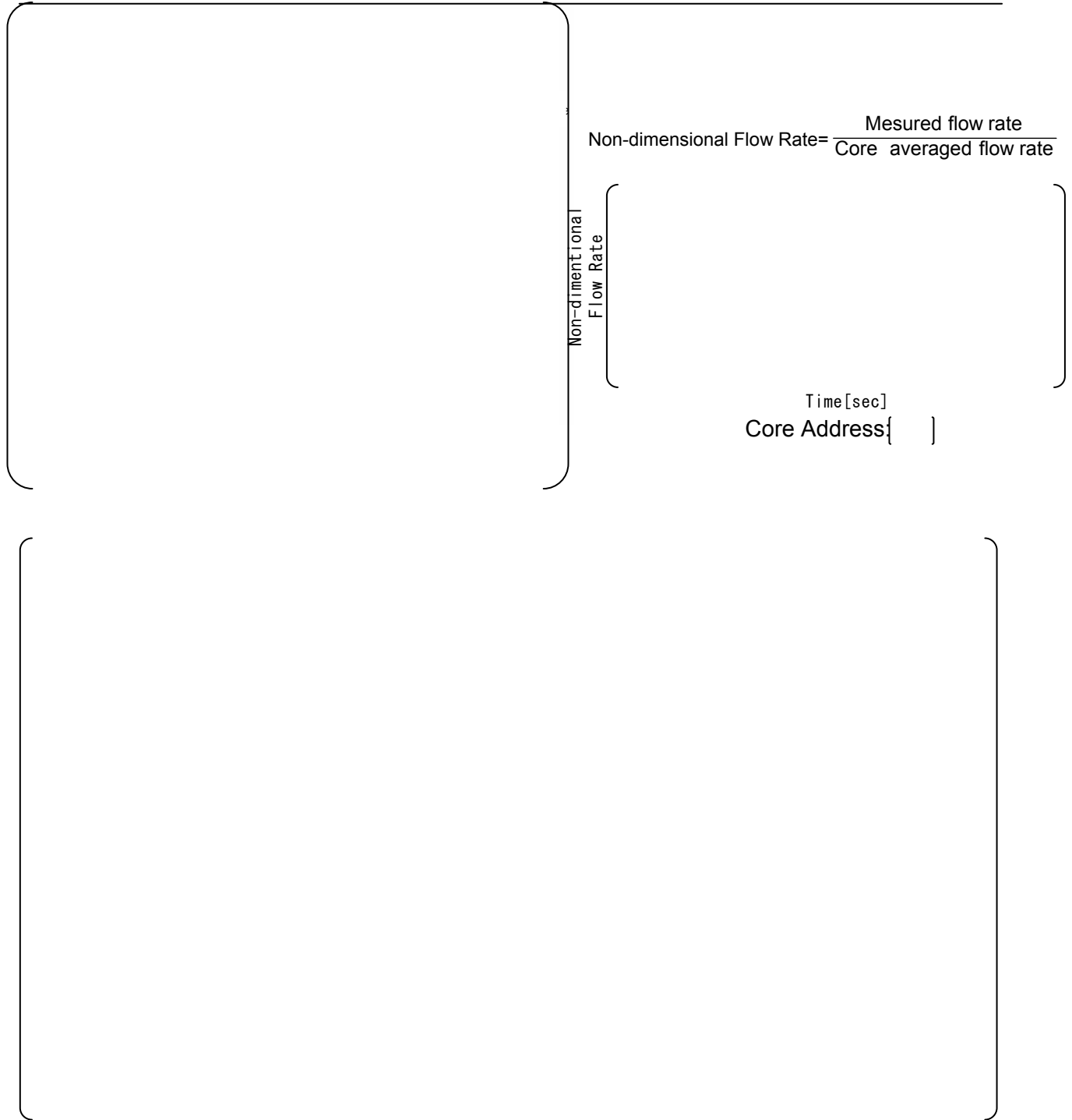


Figure 4-9 Time History of Flow Rate Distribution (with Diffuser Plate Assembly and Design LCSP Flow Hole Pattern: Test H3)



Non-dimensional Flow Rate (NDFR) = Measured Flow Rate / Core Averaged Flow Rate

Figure 4-10 Core Inlet Flow Distribution (without Diffuser Plate Assembly: Test H1)



Non-dimensional Flow Rate (NDFR) = Measured Flow Rate / Core Averaged Flow Rate

**Figure 4-11 Core Inlet Flow Distribution (with Diffuser Plate Assembly: Test H2,
[])**



Non-dimensional Flow Rate (NDFR) = Measured Flow Rate / Core Averaged Flow Rate

**Figure 4-12 Core Inlet Flow Distribution (with Diffuser Plate Assembly and Design LCSP
Flow Hole Pattern: Test H3, [])**



Non-dimensional Flow Rate (NDFR) = Measured Flow Rate / Core Averaged Flow Rate

**Figure 4-13 Core Inlet Flow Distribution (with Diffuser Plate Assembly and Design LCSP
Flow Hole Pattern: Test H3, [])**



Non-dimensional Flow Rate (NDFR) = Measured Flow Rate / Core Averaged Flow Rate

**Figure 4-14 Core Inlet Flow Distribution (with Diffuser Plate Assembly and Design LCSP
Flow Hole Pattern: Test H3, N-1 Loop)**

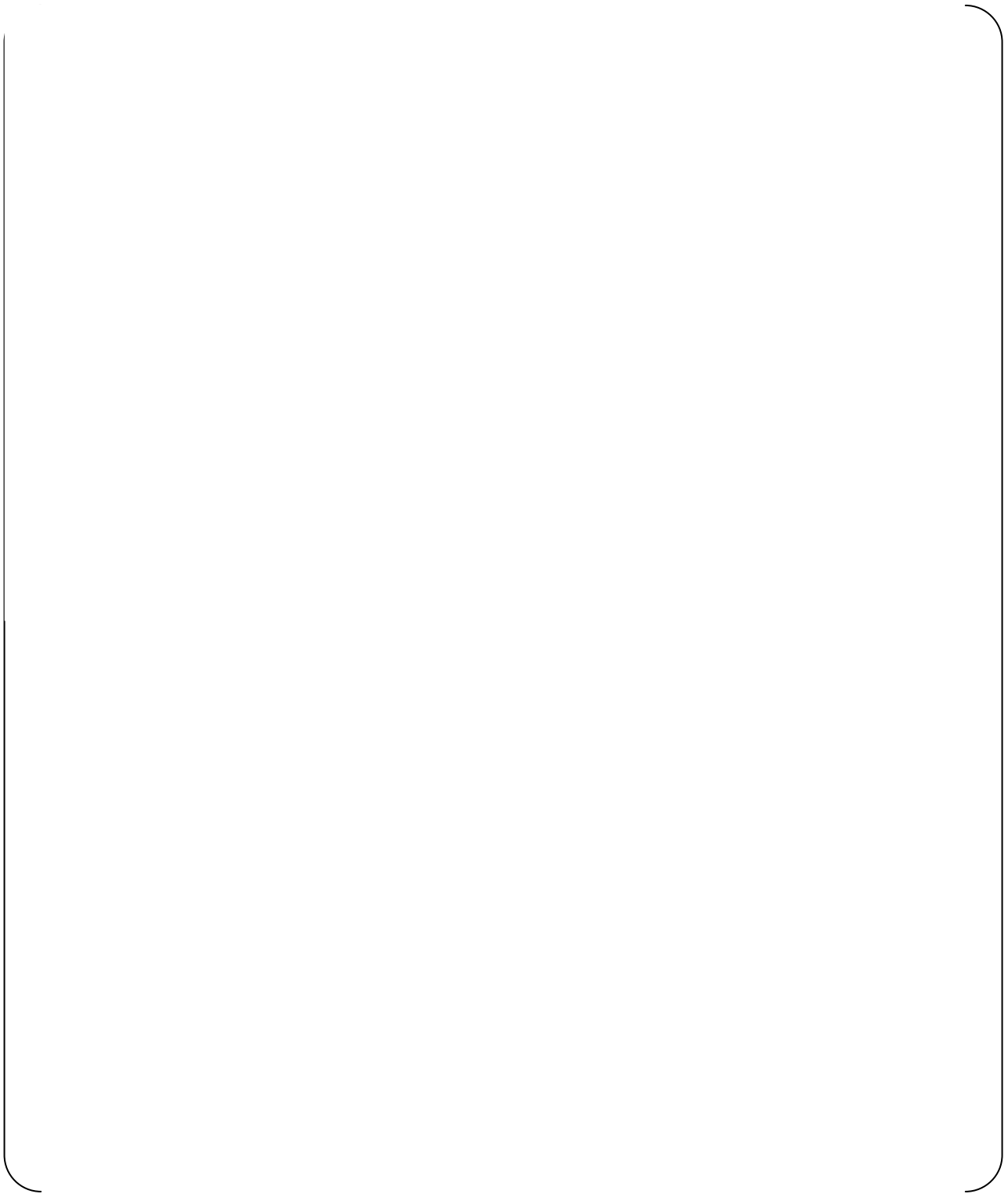


Figure 4-15 Measured Pressure Losses (Dependency with Re Number: Test H3)

	Measuring and Tapping Locations	Reference of Mode Shape
<p>Upper Diffuser Plate Subassembly</p>		
<p>Lower Diffuser Plate Subassembly</p>		

Figure 4-16 Measuring and Tapping Locations and Reference of Mode Shape

		Natural Frequency (Hz)	Vibration Mode
Upper Diffuser Plate Subassembly	Transversal Mode []		
	Rotational Mode		
	Oval Mode		
Lower Diffuser Plate Subassembly	Transversal Mode []		
	Rotational Mode		

Figure 4-17 Natural Frequencies and Vibration Mode Shapes

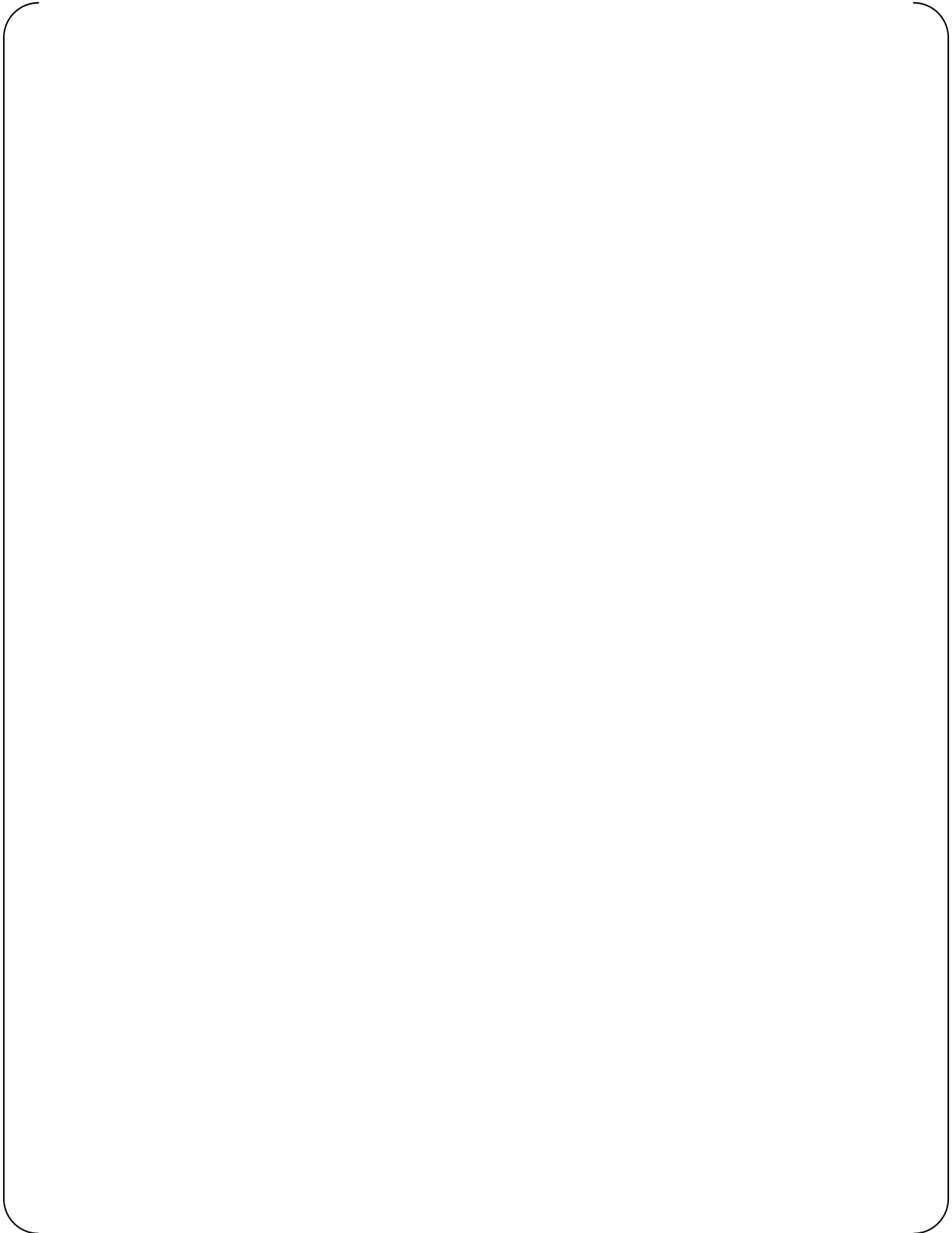


Figure 4-18 Flow Rate Dependency of Vibration Response



Figure 4-19 Core Inlet Non-dimensional Temperature Distribution



Figure 4-20 Safety Analysis Model for Core Inlet Temperature Distribution



Figure 4-21 Comparison of Core Inlet Temperature Distribution between Safety Analysis Model and Flow Test

5. CONCLUSIONS

From the results of the Reactor Vessel Lower Plenum 1/7 Scale Model Flow Tests for US-APWR, the following conclusions are drawn:

- (1) The configured design of reactor vessel lower plenum with the diffuser plate assembly and LCSP flow holes provides the core inlet flow distributions at great flow stability.
- (2) No abnormal vibration such as the lock-in vortex-induced vibration or the fluid elastic instability that is present in the components in the vessel lower plenum. The alternating stresses in the components are smaller than the design limit for the high cycle fatigue.
- (3) The core inlet temperature distribution under asymmetric loop cooling conditions is bounded by the safety analysis model on the downcomer/lower plenum mixing.

6. REFERENCES

- 1 "Design Control Document for The US-APWR Chapter4 Reactor", Table 4.1.1, UAP-DC004 Revision 0, Mitsubishi Heavy Industries, LTD., 2007.
- 2 ASME Boiler and Pressure Vessel Code Section III Division 1 Appendix I, Figure I-9.2.1 and Figure I-9.2.2, 2001 Edition, including 2003 addend.
- 3 R. D. Blevins, "Applied Fluid Dynamics Handbook", 4.4 Reynolds Number (p10), Van Nostrand Reinhold Company, 1984, ISBN:0-442-21296-8.
- 4 R. D. Blevins, "Flow-induced Vibration", 2.2.2 Reduced Velocity, Non-dimensional Amplitude (p6) , Van Nostrand Reinhold Company, 1977, ISBN:0-442-20828-6.
- 5 R. D. Blevins, "Flow-induced Vibration", 3.3 Strouhal Number ,Fig 3-3 (p15), Van Nostrand Reinhold Company, 1977, ISBN:0-442-20828-6.
- 6 J.S. Turner, "Buoyancy Effects in Fluids", p291, Cambridge at The University Press,1973
- 7 ASME Boiler and Pressure Vessel Code Section III Division 1 Appendix N, N-1300 Flow-induced Vibrations of Tubes and Tube Banks, 2001 Edition, including 2003 addend.
- 8 ASME Boiler and Pressure Vessel Code Section III Division 1, NG-3222.4 Analysis for Cyclic Operation, (2) Local Structural Discontinuities, 2001 Edition including 2003 addenda
- 9 ASME Boiler and Pressure Vessel Code Section III Part D, Subpart 2 Physical Properties Tables, Table TM-1, 2001 Edition including 2003 addenda.
- 10 J. Ogawa, et al., "Non-LOCA Methodology", MUAP-07010-P, Mitsubishi Heavy Industries, LTD., 2007

APPENDIX - 1

Response to the Request for Additional Information on US-APWR Vessel Lower Plenum 1/7 Scale Model Flow Test plan (UAP-HF-07080-P rev.0)

1. The scale model tests would be conducted in an inverted. Provide justification to show that the gravitational and other orientation effects would have negligible influence on the test results or that these effects would be accounted for and the test results would be adjusted accordingly.

(Answer 1)

In general, gravity effects on the fluid flow are limited in the case of free surface or non-uniform mass density distribution. In all cases of US-APWR lower plenum testing, there is no fluid free surface in the test vessel and the inlet pipes. As for the hydraulic test and the flow-induced vibration test, fluid mass density is uniform. Therefore, even in the inverted condition, there is no effect by gravity on the flow conditions in the hydraulic test and the flow induced vibration test.

In the temperature distribution test, the non-uniform mass density condition is generated to simulate the event with overcooling.

The fluid temperature in the event loop will be lower than the other three loops in the actual plant, thus, the direction of buoyancy on the overcooling fluid is downward. This is same with the down comer flow direction.

In the test, the hot water is injected to the event inlet pipe to minimize the hot water tank volume. Hence, the direction of the buoyancy on the injected hot water is upward, which coincides with the down-comer flow direction. Therefore, the inverted condition is qualitatively better for the simulation of the buoyancy effects. Further discussion with non-dimensional parameter Ri will be discussed in the answer to the question 2.

2. The tests would be conducted at room temperature on a 1/7 scale model. The results of a non dimensional analysis to show that tests under these conditions accurately simulate the flow induced vibrations are summarized in Table 4-3. Provide the basis for the selection of the non dimensional parameters and discuss how these are sufficient to accurately simulate the flow induced vibration responses.

(Answer 2)

The Reynolds number Re for the hydraulic test and the reduced velocity U_r for the flow-induced vibration test are selected as the key non-dimensional parameters. In addition for the temperature distribution test, Richardson number Ri is evaluated to check the buoyancy

effects on the temperature mixing. Definitions and bases of these non-dimensional parameters are summarized in Table 1 and discussed below.

a. Hydraulic test

$Re (=UD/\nu)$ based on flow path dimension, as described in Ref.(1), is a measure to check if the simulation of the turbulent flow condition is maintained. Because the transition from the laminar flow to the turbulent flow occurs at Re of order of 10^3 , we have set the criteria at 10^4 . This requirement is needed not only for the hydraulic test, but also for the flow induced vibration test and for temperature distribution test.

At nominal conditions for the hydraulic test, Re at the down-comer is 2×10^5 . It remains of order of 10^5 even in minimum flow conditions. These values are sufficiently high to simulate the full developed turbulent flow conditions as in actual plant.

b. Flow-induced vibration test

The reduced velocity $Ur (= U/f_n D)$ is generally utilized in the dimension analysis of flow induced vibration. Ur represents the ratio of the path length per cycle (U/f_n) and the model width D as described in Ref.(2). From another view, Ur represents the ratio of the fluid force frequency (proportional to U/D , the vortex shedding frequency f_s is a typical example) and the model natural frequency. The nominal flow rate in the test should be determined as Ur coincides with that of the plant. If the test model is precisely scaled downed, " $f_n D$ " is maintained. Therefore, same velocity is the answer for coincidence of Ur with the plant condition.

The effects of temperature condition on flow induced responses are considered from the view point of flow induced forcing function and stiffness of structure. The main source of flow induced vibration is the turbulence pressure fluctuation and second is vortex shedding. The amplitude of these forcing functions are in proportion with the dynamic pressure ($=1/2\rho U^2$), thus, the temperature effect on the flow induced forces can be related to the change of fluid mass density. As for the effect on the structure stiffness, it can be estimated from the ratio of Young's modulus of the material. Therefore, the effect of temperature on vibration response will be corrected with the difference of fluid mass density and the difference of Young's modulus. Total correction factors including scale effects are summarized in Table 2.

c. Temperature distribution test

As discussed in answer 1, the buoyancy effects on temperature mixing is checked by applying the Richardson number Ri . Ri is a non-dimensional parameter which represents the ratio of buoyancy and fluid inertia forces as described in Ref.(3). In both actual plant event conditions and in test conditions, Ri are much smaller than 1.0. This means that the buoyancy effects on temperature mixing is negligibly small, and temperature mixing can be simulated in the test conditions.

3. MNES is requested to provide the number and length of test runs that will be performed for each of the three tests. In addition, MNES is requested to submit the test results to the NRC staff.

(Answer 3)

The number of test runs and measurement time duration for the hydraulic test, FIV test, and the temperature distribution test are shown in Table 3.

The test report will be submitted to NRC by the end of June 2008.

Table 1 Non-dimensional Parameters

	Definition	Bases	Test Requirement	Actual Plant (Approx.)	Test Condition (Approx.)
Hydraulic Test	$Re=UD_1/\nu$	Ratio of fluid Inertia force and viscous force	$Re \gg 10^4$ (for developed turbulent flow)	{	}
FIV Test	$Ur = U / fn D_2$	Ratio of "path per cycle" and "model width"	Equivalent with plant condition		
Temp. Distribution test	$Ri = \frac{gD_1(\delta\rho)}{\rho V^2}$	Ratio of buoyancy and fluid inertia force	Equivalent with plant condition or $Ri \ll 1.0$ for test and plant		

- U: flow velocity (= down-comer average velocity)
- D_1 : typical length of the flow path (= down-comer width)
- D_2 : typical length of the structure (= diameter of diffuser plate support column)
- ν : kinematic viscosity
- fn : natural frequency
- g : gravity acceleration
- ρ : fluid mass density
- $\delta\rho$: difference of mass density between cold fluid and hot fluid

Table 2 Correction Factors for FIV Test Results (Approx.)

	Effect of Temperature		Scale Factor (1/7 Scale)	Total Correction Factor
	Correction for Fluid Mass Density	Correction for Young's Modulus		
Hydraulic Force	0.75	NA	49	37
Stress	0.75	NA	1/1	0.75
Natural Frequency	1.01	0.95	1/7	0.14
Displacement	0.75	1.1	7	5.8
Acceleration	0.77	NA	1/7	0.11

Table 3 Number of Test Runs and Duration

	ID	Structures in Lower Plenum	LCSP(*1) Flow Hole Orifice	Loop Flow Rate	Number of Test Runs (*2)	Test Duration (per Run)		
Hydraulic Test	H1							
	H2							
	H3							
FIV Test	F1							
	F2							
	F3							
	F4							
	F5							
Temp Distribution Test	T1							

*1: LCSP = Lower Core Support Plate

*2: + means additional run to check the repeatability

References

- (1) Robert D. Blevins, "Applied Fluid Dynamics Handbook", 4.4 Reynolds Number (p10) , Van Ostrand Reinhold Company, 1984, ISBN:0-442-21296-8
- (2) Robert D. Blevins, "Flow-Induced Vibration", 2.2.2 Reduced Velocity, Nondimensional Amplitude (p6) , VAN OSTRAND REINHOLD COMPANY, 1977, ISBN:0-442-20828-6
- (3) J. S. Turner, "Buoyancy Effects in Fluids", p291, Cambridge at the University Press, 1973

APPENDIX - 2

Evaluation of Measurement Uncertainties

1. INTRODUCTION

The evaluation of measurement uncertainties was performed for the quantitative evaluation results of the 1/7-scale model flow test for the reactor vessel lower plenum. This test was conducted to confirm the thermal hydraulic and flow-induced vibration characteristics of the US-APWR lower plenum design.

The measurement uncertainties were evaluated for the measured results of the core inlet flow distribution, the neutron reflector inlet flow distribution, the pressure loss, flow-induced vibration and the temperature distribution in the 1/7-scale model flow test.

This appendix provides the summary of the evaluation effort.

2. EVALUATION CONTENTS OF MEASUREMENT UNCERTAINTIES

2.1 Evaluation Items of Measurement Uncertainties

The evaluation of measurement uncertainties were based on the GUM (Guide to the Expression of Uncertainty in Measurement) (Ref. 1) which was published by International Organization for Standardization.

The measurement uncertainties were composed of the uncertainties of the loop flow rate, the measurement system, and the dispersion of the measured data.

The uncertainty of the loop flow rate was composed of the uncertainties of the orifice, the flow rate measurement system, and the estimated fluid density.

The uncertainty of the measurement system can be deduced based on the specifications of the data processing system and the instrumentations such as the sensors, the universal

recorder with the amplifier and the A/D converter. These uncertainties were evaluated by the calibration tests for the measurement system.

The dispersion of measurement data is caused by the intrinsic fluctuation existing in the actual flow, such as turbulence and unsteadiness of flow. The uncertainties of measured data were obtained from the repeated data measurement. These uncertainties were evaluated according to the following procedure.

2.2 Statistical Method

In the evaluation procedure based on the GUM, the expanded uncertainty U is derived by multiplying the combined standard uncertainty by the coverage factor. The expanded uncertainty means an interval about the measurement result that may be expected to encompass a large fraction of the distribution of measured values.

The combined standard uncertainty is estimated as the square root of the sum of the square of the standard uncertainties. The uncertainty expressed as standard deviation is called the standard uncertainty. The standard uncertainty is composed of the uncertainties of the flow rate setting and the measurement system and the dispersion of the measured data.

The expanded uncertainty and the combined standard uncertainty are derived by the following equations.

$$U = ku_C$$

$$u_C = \sqrt{\sum_i (u_i)^2}$$

U : Expanded uncertainty

k : Coverage factor

u_C : Combined standard uncertainty

u_i : Standard uncertainty

The number of the coverage factor k was selected as $k = [\quad]$ which produces an interval having a level of confidence of approximately $[\quad]$ percent.

Relative expanded uncertainty $U/|Y|$, relative combined standard uncertainty $u_c/|Y|$ and relative standard uncertainty $u_i/|Y|$ were used to evaluate the ratio of the measurement uncertainty to the measured value. The data $|Y|$ are the absolute numbers of the measured data.

3. EVALUATION OF MEASUREMENT UNCERTAINTIES

3.1 Core Inlet Flow Distribution

The block diagram of the core inlet flow distribution measurement is shown in Figure A3-1. In this measurement, the [] differential pressure transducers were used to measure the core inlet flow distribution. These transducers were connected with the Venturi flow meters mounted on the core inlet. The [] differential pressure transducers were used to measure the loop flow rate. These transducers were connected with the orifice located in all inlet pipes.

The combined uncertainty was composed of the uncertainties of the flow rate measurement system, the average core inlet flow rate, and the dispersion of the measured data. The uncertainty of the flow rate setting was not considered. This was because the core inlet flow distribution was evaluated by using the reduced flow rate divided by the average core inlet flow rate.

(a) Measurement system

The uncertainty of flow rate measurement system was composed of the uncertainties of the Venturi flow meters, the [] differential pressure transducers, and the universal recorders with the A/D converters. These uncertainties were obtained from the calibration tests for the Venturi flow meters and the catalogs of the transducers and the recorders. The average standard uncertainty of the measurement system was [] percent.

(b) Average core inlet flow rate

The core inlet flow distribution was evaluated by using the reduced flow rate divided by the average core inlet flow rate of the [] measured data. This evaluation was affected by the average core inlet flow rate. Therefore, the uncertainty of this average core inlet flow

rate was also evaluated. The standard uncertainty of the average core inlet flow rate was [] percent.

(c) Dispersion of measured data

The uncertainty of the measured data was obtained from the reduced flow rates measured at []. The average standard uncertainty of the dispersion of measured data was [] percent.

(d) Conclusion

The uncertainty in the core inlet flow distribution measurement is shown in Table A3-1. The combined standard uncertainty of the core inlet flow distribution measurement is [] percent. The expanded uncertainty is [] percent if the coverage factor k is selected as $k = []$, which produces an interval having a level of confidence of approximately [] percent.

For the maximum differential flow rate between adjacent fuel assemblies, the uncertainty can be estimated as the convolution of uncertainties for two assemblies flow rates. So the expected uncertainty with [] percent confidence is [] percent.

3.2 Neutron Reflector (NR) Inlet Flow Distribution

The block diagram of the NR inlet flow distribution measurement is shown in Figure A3-2. In this process the [] differential pressure transducers were used to measure the NR inlet flow distribution. These transducers were connected with the Venturi flow meters mounted on the NR inlet. The [] differential pressure transducers were used to measure the loop flow rate. These transducers were connected with the orifice located in all inlet pipes.

The combined uncertainty was composed of the uncertainties of the flow rate setting, the measurement system, and the dispersion of the measured data. The uncertainty of the loop flow rate was considered. This was because the NR inlet flow distribution was evaluated by using the reduced flow rate divided by the design value of the total NR inlet flow rate. This was calculated from the total loop flow rate measured at all inlet pipes.

(a) Loop flow rate

The block diagram of the flow-induced vibration measurement is shown in Figure A3-4. In the flow-induced vibration test, the [] strain gages mounted on the diffuser support column were used to evaluate flow induced vibration.

The combined uncertainty was composed of the uncertainties of the flow rate setting, the strain measurement system, and the dispersion of the measured data.

(a) Flow rate setting

The uncertainty of flow rate setting was composed of the uncertainties of the orifice, the measurement system, estimated fluid density, and the dispersion of flow rate data measured at []. The standard uncertainty of the flow rate setting was [] percent.

(b) Measurement system

In the flow-induced vibration measurement, the strain data of the diffuser support columns, the acceleration data of the diffuser plates, impact force data, and the pressure fluctuation data at the downcomer and lower plenum were measured.

The acceleration data and the impact force data were used for the identification of the natural frequencies and vibration mode shapes. The pressure fluctuation data were used for monitoring the dominant frequency of the pressure fluctuation in the flow-induced vibration measurement. The strain data were used for the evaluation of the absence of the abnormal vibration and the evaluation of the high cycle fatigue. Therefore, the uncertainty of only the strain data was presented in this appendix.

The uncertainty of the strain measurement system in the flow-induced vibration measurement was composed of the uncertainties of the standard strain generator, the strain amplifiers and the data recorders with the A/D converters. These uncertainties were obtained by the calibration tests. The average standard uncertainty of the strain measurement system was [] percent.

(c) Dispersion of measured data

The uncertainty of measured data was obtained from the stress data measured [] times at [] used for the high cycle fatigue evaluation. The average standard uncertainty of the dispersion of measured data was [] percent.

(d) Conclusion

The uncertainty of the strain measurement system is shown in Table A3-4. The combined standard uncertainty of the system is [] percent. The expanded uncertainty is [] percent if the coverage factor k is selected as $k = []$, which produces an interval having a level of confidence of approximately [] percent.

3.5 Core Inlet Temperature Distribution Measurement

The block diagram of the core inlet temperature distribution measurement is shown in Figure A3-5. In this measurement, [] thermocouples were mounted on the core inlet to measure the temperature distribution and [] thermocouples were used to measure the loop temperature.

The combined uncertainty was composed of the uncertainties of the measurement system and the dispersion of the measured data.

(a) Measurement system

The uncertainty of core inlet temperature distribution measurement was composed of the uncertainties of the thermocouples and the universal recorders with A/D converters. These uncertainties were obtained from the catalogs of the thermocouples and the recorders. The average standard uncertainty of the measurement system was [] percent.

(b) Dispersion of measured data

The uncertainty of measured data was obtained from the temperature data measured twice at []. The average standard uncertainty of the dispersion of measured data was [] percent.

(c) Conclusion

The uncertainty in the core inlet temperature distribution measurement is shown in Table A3-5. The combined standard uncertainty of the core inlet temperature distribution measurement is [] percent. The expanded uncertainty is [] percent if the coverage factor k was selected as $k = []$, which produces an interval having a level of confidence of approximately [] percent.

Table A3-1 Uncertainties in Core Inlet Flow Distribution Measurement

Item	$u_i/ Y $ (percent)	$u_C/ Y $ (percent)
Measurement system	{	}
Average core inlet flow rate		
Measured data		

Table A3-2 Uncertainty in Measurement of NR Inlet Flow Distribution

Item	$u_i/ Y $ (percent)	$u_C/ Y $ (percent)
Loop flow rate	{	}
Measurement system		
Measured data		

Table A3-3 Uncertainty in Pressure Loss Measurement

Item	$u_i/ Y $ (percent)	$u_C/ Y $ (percent)
Loop flow rate	{	}
Measurement system		
Measured data		

Table A3-4 Uncertainty in Flow-induced Vibration Measurement

Item	$u_i/ Y $ (percent)	$u_C/ Y $ (percent)
Flow rate setting	[]
Measurement system		
Measured data		

Table A3-5 Uncertainty in Core Inlet Temperature Distribution Measurement

Item	$u_i/ Y $ (percent)	$u_C/ Y $ (percent)
Measurement system	[]
Measured data		

Figure A3-1 Block Diagram of Core Inlet Flow Distribution Measurement

Figure A3-2 Block Diagram of Measurement of NR Inlet Flow Distribution

Figure A3-3 Block Diagram of Pressure Loss Measurement



Figure A3-4 Block Diagram of Flow-induced Vibration Measurement



Figure A3-5 Block Diagram of Core Inlet Temperature Distribution Measurement

4. REFERENCE

(1) Guide to the expression of uncertainty in measurement (GUM), ISO/IEC Guide 98:1995.